believe that vitreoretinal traction is an important factor in the pathogenesis of macular detachment associated with an optic disc pit, we feel that vitrectomy with complete PVD induction is essential for the treatment of these eyes. We postulate that vitreous traction may play a critical role in the development of these detachments, although we were unable to detect any vitreomacular or vitreopapillary traction by OCT. The added use of gas tamponade probably helps to push fluid from the inner layer separation into the outer layer detachment. Because we did not apply laser photocoagulation at the optic disc pit margin in our patients, we deduce that release of continued vitreoretinal traction by surgical induction of PVD was sufficient to lead to diminishment of new fluid accumulation in the inner layer separation presumably coming from the optic disc pit. This idea is supported by our postoperative OCT findings in patient 10, showing that the inner layer separation resolved first, before resolution of the outer layer detachment.

Vitrectomy with gas tamponade, with or without laser application to the margin of the pit, for macular detachment associated with an optic disc pit has been reported.[12–14] However, these series did not achieve VA results as good as those of the current study, and had higher rates of reoperation. This difference may be due to differences in surgical technique. Furthermore, the current study did not employ any laser application to achieve good visual and anatomical outcomes, and we believe that assuring a complete PVD induction during surgery played an integral part in achieving these results.

Favorable visual and anatomical outcomes have also been reported using macular buckling in Theodossiadis's series of 9 consecutive patients with optic disc pit maculopathy.[16] Recently, Theodossiadis and Theodossiadis have also reported on OCT findings in 26 eyes treated with scleral buckling, with resolution of macular detachment noted in 24 eyes. Disappearance of intraretinal fluid over 7 to 9 months postoperatively was documented in 4 of 5 eyes that were evaluated by OCT both before and after surgery.[27] We believe that these favorable results with scleral buckling are due to conversion of the inward perpendicular component of the vector, caused by tangential forces associated with posterior hyaloid traction on the retina at the irregular surface of the optic disc, to an outward perpendicular vector component by the scleral buckle promoting attachment of the retina.[28]

Spontaneous resolution of the macular detachment associated with optic nerve pits is also known to occur in approximately 25% of untreated patients.[4] However, cystic retinal degeneration, macular hole formation, and retinal pigment epithelial atrophy often limit visual recovery in these cases. Over half of eyes with macular detachments experience a decrease in VA to 20/100 or less within 5 years.[3] In contrast, although the time to best VA took close to 6 months in most patients, 9 of 11 eyes eventually achieved a postoperative VA of 0.8 or greater. Furthermore, we found that VA started to improve after surgery despite the continued, albeit decreased, presence of inner layer separation and outer layer detachment in the fovea by OCT. This suggests that mild improvements in foveal contour alone may lead to improved vision and that long-term observation is essential postoperatively in these eyes. In eyes that have undergone vitrectomy, additional treatments for the macular detachment should not be contemplated too early. Furthermore, given the fact that subretinal fluid persisted for a long time postoperatively but eventually resolved, gas tamponade may actually not be necessary for successful treatment. Because all eyes in the current study received gas tamponade, we are not able to assess this possibility.

Complications associated with surgery included VF defects in 2 of 11 eyes, both of which were early cases in our series. We believe that improved surgical technique allowed us to avoid such complications in later cases.[29,30] Because the induction of PVD in young eyes is particularly difficult, due to strong vitreoretinal adhesion, special care must always be taken to avoid excessive mechanical damage when separating the posterior hyaloid from the optic disc and posterior pole. A longer duration of surgery may also lead to an increased risk of light toxicity, as has been reported in macular hole surgery.[29–31] However, surgery-related insults must also be distinguished from VF aberrations that may be present preoperatively in these eyes with optic disc pits.

In conclusion, vitrectomy with modern surgical techniques for creating PVD in young patients and gas tamponade, without laser photocoagulation, can lead to successful reattachment of the macula and improvement in central vision in eyes with optic disc pit maculopathy, although most eyes required almost 1 year to reach this state.

References

1. Wiethe T. Ein fall von angeborener Difformität der Sehnervenpapille. Arch Augenheilkd 1882;11:14–9.
2. Kranenburg EW. Crater-like holes in the optic disc and central serous retinopathy. Arch Ophthalmol 1960;64:912–24.
3. Brown GC, Shields JA, Goldberg RE. Congenital pits of the nerve head. II. Clinical studies in humans. Ophthalmology 1980;87:51–65.
4. Sobol WM, Blodi CF, Folk JC, Weingeist TA. Long-term visual outcome in patients with optic nerve pit and serous retinal detachment of the macula. Ophthalmology 1990;97:1539–42.
5. Lincoff H, Lopez R, Kreissig I, et al. Retinoschisis associated with optic nerve pits. Arch Ophthalmol 1988;106:61–7.
6. Rutledge BK, Puliafito CA, Duker JS, et al. Optical coherence tomography of macular lesions associated with optic nerve head pits. Ophthalmology 1996;103:1047–53.
7. Krivoy D, Gentile R, Liebmann JM, et al. Imaging congenital optic disc pits and associated maculopathy using optical coherence tomography. Arch Ophthalmol 1996;114:165–70.
8. Lincoff H, Kreissig I. Optical coherence tomography of pneumatic displacement of optic disc pit maculopathy. Br J Ophthalmol 1998;82:367–72.
9. Gass JDM. Serous detachment of the macula: secondary to congenital pit of the optic nervehead. Am J Ophthalmol 1969;67:821–41.
10. Gass JDM. Stereoscopic Atlas of Macular Diseases: Diagnosis and Treatment. Vol. II. 3rd ed. St. Louis: Mosby; 1987:728–33.
11. Tobe T, Nishimura T, Uyama M. Laser photocoagulation for pit-macular syndrome [in Japanese]. Ganka Rinshoiho 1991;85:124–30.

12. Cox MS, Witherspoon CD, Morris RE, Flynn HW. Evolving techniques in the treatment of macular detachment caused by optic nerve pits. Ophthalmology 1988;95:889–96.
13. Postel EA, Pulido JS, McNamara JA, Johnson MW. The etiology and treatment of macular detachment associated with optic nerve pits and related anomalies. Trans Am Ophthalmol Soc 1998;96:73–88.
14. Mitamura Y, Takeuchi S, Tsukahara I, et al. Vitreous surgery in two cases of pit-macular syndrome [in Japanese]. Rinsho Ganka 1997;51:251–4.
15. Snead MP, James N, Jacobs PM. Vitrectomy, argon laser, and gas tamponade for serous retinal detachment associated with an optic disc pit: a case report. Br J Ophthalmol 1991;75: 381–2.
16. Theodossiadis GP. Treatment of maculopathy associated with optic disk pit by sponge explant. Am J Ophthalmol 1996;121: 630–7.
17. Lincoff H, Yanuzzi L, Singerman L, et al. Improvement in visual function after displacement of the retinal elevations emanating from optic pits. Arch Ophthalmol 1993;111:1071–9.
18. Bonnet M. Serous macular detachment associated with optic nerve pits. Graefes Arch Clin Exp Ophthalmol 1991; 229:526–32.
19. Gordon R, Chatfield RK. Pits in the optic disc associated with macular degeneration. Br J Ophthalmol 1969;53:481–9.
20. Kelly NE, Wendel RT. Vitreous surgery for idiopathic macular holes. Results of a pilot study. Arch Ophthalmol 1991; 109:654–9.
21. Lewis H, Abrams GW, Blumenkranz MS, Campo RV. Vitrectomy for diabetic macular traction and edema associated with posterior hyaloidal traction. Ophthalmology 1992;99: 753–9.
22. Tachi N, Ogino N. Vitrectomy for diffuse macular edema in cases of diabetic retinopathy. Am J Ophthalmol 1996;122: 258–60.
23. Peyman GA, Cheema R, Conway MD, Fang T. Triamcinolone acetonide as an aid to visualization of the vitreous and the posterior hyaloid during pars plana vitrectomy. Retina 2000; 20:554–5.
24. Sakamoto T, Miyazaki M, Hisatomi T, et al. Triamcinolone-assisted pars plana vitrectomy improves the surgical procedures and decreases the postoperative blood-ocular barrier breakdown. Graefes Arch Clin Exp Ophthalmol 2002;240: 423–9.
25. Griffiths MFP. The use of fluorescein in vitrectomy [letter]. Arch Ophthalmol 1987;105:889.
26. Girard LJ. Fluorescein staining of formed vitreous to aid in vitrectomy [letter]. Ophthalmic Surg 1984;15:874.
27. Theodossiadis GP, Theodossiadis PA. Optical coherence tomography in optic disk pit maculopathy treated by the macular buckling procedure. Am J Ophthalmol 2001;132:184–90.
28. Michels RG, Thompson JT, Rice TA, Freund D. Effect of scleral buckling on vector forces caused by epiretinal membranes. Am J Ophthalmol 1987;104:667–70.
29. Pendergast SD, McCuen BW II. Visual field loss after macular hole surgery. Ophthalmology 1996;103:1069–77.
30. Ohji M, Nao-I N, Saito Y, et al. Prevention of visual field defect after macular hole surgery by passing air used for fluid-air exchange through water. Am J Ophthalmol 1999;127: 62–6.
31. Michels M, Lewis H, Abrams GW, et al. Macular phototoxicity caused by fiberoptic endoillumination during pars plana vitrectomy. Am J Ophthalmol 1992;114:287–96.

Cell Tissue Res (2006) 325: 101–109
DOI 10.1007/s00441-005-0122-z

REGULAR ARTICLE

Yasuko Yamaguchi · Takashi Watanabe ·
Akito Hirakata · Tetsuo Hida

Localization and ontogeny of aquaporin-1 and -4 expression in iris and ciliary epithelial cells in rats

Received: 7 August 2005 / Accepted: 8 November 2005 / Published online: 7 March 2006

Abstract The precise localization of aquaporin (AQP)1 and AQP4 was studied in iris and ciliary epithelial cells, in both mature and developing rats, to elucidate the molecular mechanisms underlying aqueous humor balance. Anterior segments of eyes dissected from embryonic day (E)13, E15, E18, and E20, postnatal day (P)0, P7, and P14, and postnatal week 8 rats were subjected to immunofluorescence analysis with AQP isoform-specific antibodies. In adult rat eye, AQP1 was localized to the apical and basolateral plasma membranes of iris epithelial cell layers and of anterior ciliary non-pigmented epithelial (NPE) cells. Conversely, AQP4 was localized to the basolateral plasma membrane of NPE cells in ciliary epithelium and the posterior iris. Developmentally, AQP1 was detected as early as E15 in immature iris and ciliary epithelial cells, and expression persisted throughout development up to adulthood. In contrast, AQP4 was first observed at P7 in the developing pars plicata, and the AQP4-positive area gradually spread to cover the entire pars plicata as development proceeded. These findings indicate that both AQP1 and AQP4 contribute to aqueous humor secretion in the rat eye, thereby maintaining proper intraocular pressure. Moreover, AQP appears to play a major role in aqueous humor secretion in early eye development. This study thus provides a basis for understanding the molecular mechanisms of aqueous humor secretion in pathological and physiological conditions.

Keywords Aquaporin · Iris epithelium · Ciliary epithelium · Aqueous humor · Fluid transport · Immunofluorescence analysis · Rat (Sprague Dawley)

Y. Yamaguchi (✉) · A. Hirakata · T. Hida
Department of Ophthalmology,
Kyorin University School of Medicine,
6-20-2 Shinkawa,
Mitaka, Tokyo, 181-8611, Japan
e-mail: yamaguchi@eye-center.org
Tel.: +81-422-475511

T. Watanabe
Laboratory Medicine,
Kyorin University School of Medicine,
6-20-2 Shinkawa,
Mitaka, Tokyo, 181-8611, Japan

Introduction

Aquaporins (AQPs) are molecular water channels localized in plasma membranes in animals, plants, and microorganisms (Chrispeels and Agre 1994; Calamita et al. 1995). In mammalian cells, 11 isoforms of AQPs (AQP0–AQP10) have been identified to date (Matsuzaki et al. 2002; Verkman 2003). AQPs are present in cells requiring either rapid bulk transport of fluid or transport of fluids against an insufficient osmotic pressure gap. AQPs allow efficient transport of fluid, thereby contributing to the maintenance of proper organ function (Stamer et al. 1994; Patil et al. 1997a; Hamann et al. 1998).

Of the 11 AQP isoforms, AQP0, AQP1, AQP3, AQP4, and AQP5 have been shown to be localized in mammalian eyes (Patil et al. 1997a; Hamann et al. 1998; Verkman 2003). AQP1 and AQP4 are localized in ciliary epithelial cells and appear to be involved in aqueous humor secretion (Patil et al. 1997a, 2001; Hamann et al. 1998; Zhang et al. 2002; Verkman 2003). Within the eye, the watery aqueous humor plays important roles in maintaining proper visual function. Aqueous humor generates a suitable intraocular pressure (IOP) and also conveys nutrients and metabolic waste to and from avascular intraocular tissues such as the lens (Caprioli 1992). Moreover, the aqueous humor appears essential in normal eye development (Reichman and Beebe 1992). Aqueous humor is also important ophthalmologically, as impairments in water dynamics can result in eye disorders such as glaucoma. The molecular

mechanisms involved in aqueous humor dynamics, however, remain largely unclear. The present study has therefore attempted to identify localization of AQP1 and AQP4 in iris and ciliary epithelial cells in rats by using immunocytochemical methods. Developmental expression of AQP1 and AQP4 in rat iris and ciliary epithelial cells has also been examined from embryonic to postnatal stages. This is the first precise analysis of AQP1 and AQP4 localization in iris and ciliary epithelial cells in both mature and developing rats.

Materials and methods

Animals

Timed-pregnant and postnatal Sprague-Dawley rats were obtained from Clea Japan (Tokyo, Japan). Birth usually occurred on embryonic day (E)22, which was considered as postnatal day (P)0. Samples taken on E13, E15, E18, and E20 from fetal rats, on P0, P7 and P14 from postnatal rats, and at postnatal week (PW)8 from adult female rats were

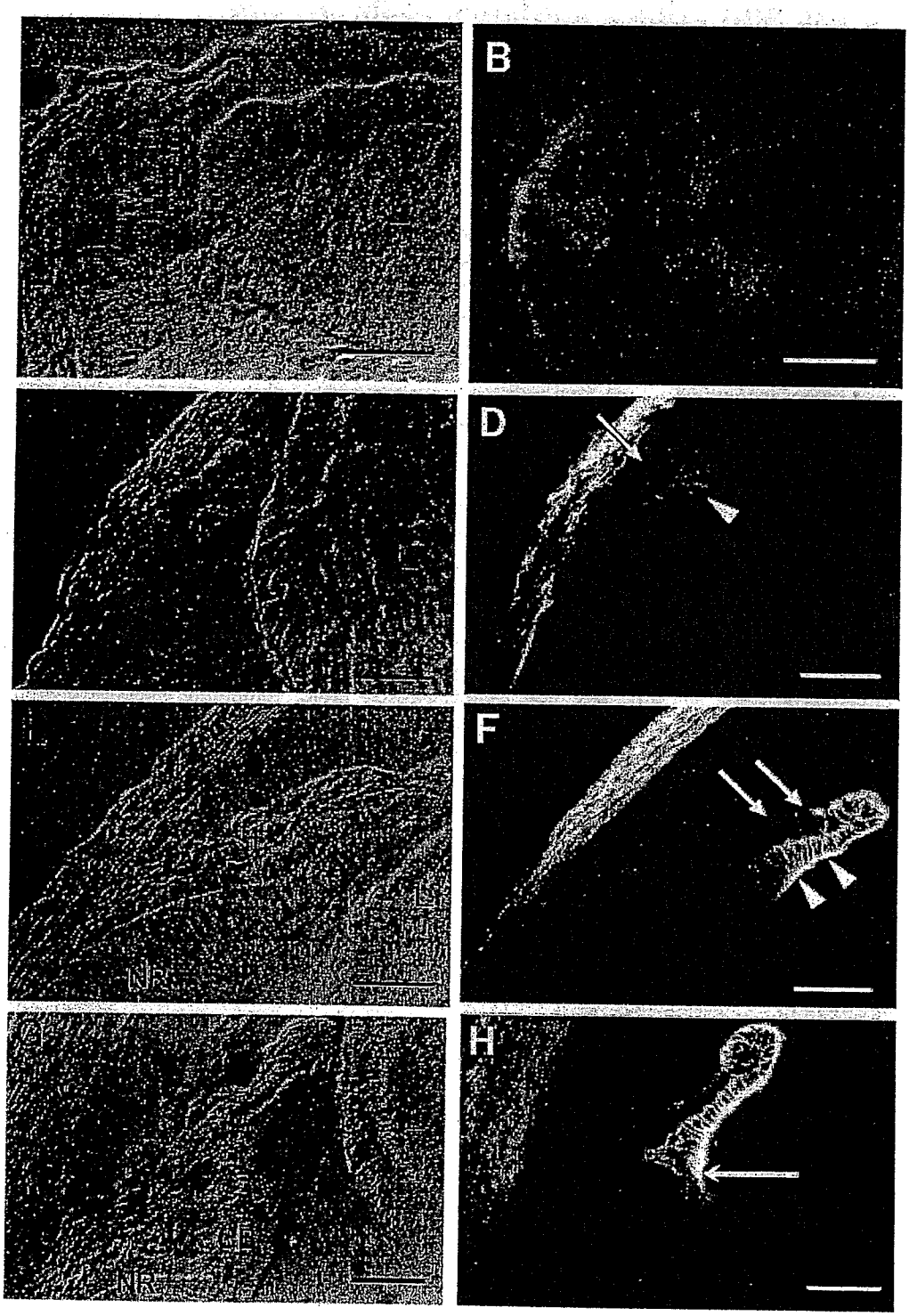

Fig. 1 AQP1 immunolocalization in iris and ciliary epithelial cells in embryonic rat eyes (*C* cornea, *L* lens, *CB* ciliary body, *NR* neural retina, *asterisks* inner plate, *stars* outer plate, *St* iris and ciliary stroma). Vertical sections through developing eyes dissected from E13, E15, E18, and E20 rats were immunostained with anti-AQP1 antibody followed by FITC-labeled swine anti-rabbit immunoglobulin and then photographed using Nomarski (**a**, **c**, **e**, **g**) and fluorescence (**b**, **d**, **f**, **h**) optics. At E13 (**a**, **b**), no definitive AQP1–IR was observed in either inner or outer plates of the optic cup. AQP1–IR first appeared at E15 (**c**, **d**). At E15 and E18 (**e**, **f**), AQP1–IR was confined to the anterior ends of the developing optic cup. Within this region, the optic cup inner plate (**d**, **f**, *arrowheads*) showed more intense AQP1–IR than the outer plate (**d**, **f**, *arrows*). The intensity of AQP1–IR increased dramatically as development proceeded from E15 (**d**) to E18 (**f**). At E20 (**g**, **h**), AQP1–IR was observed in the most anterior region of the ciliary body (**h**, *arrow*) in addition to the entire iris, and AQP1–IR intensity was significantly higher than at E15 or E18. In the cornea, AQP1–IR was first observed at E15 (**d**) and persisted throughout the embryonic stages (**f**, **h**). *Bars* 25 μm

subjected to immunohistochemical analysis. All animal care and tissue collection procedures were performed in accordance with the ARVO Statement for the Use of Animals in Ophthalmic and Vision Research.

Preparation of eye specimens

Embryos (E13, E15, E18, and E20) were removed after pregnant Sprague-Dawley rats has been killed by cervical dislocation under deep anesthesia induced by diethyl ether. Eyes were immediately enucleated and immersion-fixed in 4% paraformaldehyde in 0.1 M phosphate buffer (PB, pH 7.4) for 2 h at 4°C. Postnatal rats (P0 and P7) were sacrificed by decapitation. Eyes were immediately enucleated, and the anterior segments were dissected. Resultant eye tissues were immersion-fixed in a similar manner to embryonic eyes. For P14 and PW8 rats, animals were perfused transcardially with 0.01 M phosphate-buffered saline (PBS, pH 7.4) followed by ice-cold fixative containing 4% paraformaldehyde in PB under deep anesthesia induced by diethyl ether. Eyes were enucleated and processed in a similar manner to those from P0 and P7 rats. All tissue samples were subsequently cryoprotected by using a graded series of sucrose in PBS at 4°C, embedded in OCT compound (Sakura Finetechnical, Tokyo, Japan), and frozen. Frozen sections (6 μm) were cut in an HM500 cryostat (Zeiss) and transferred onto 3–aminopropyltrethoxy–silane–coated slides. A hydrophobic ring was drawn around sections by using a PAP pen (Daido Sangyo, Tokyo, Japan). Sections were then air-dried for 1 h at room temperature.

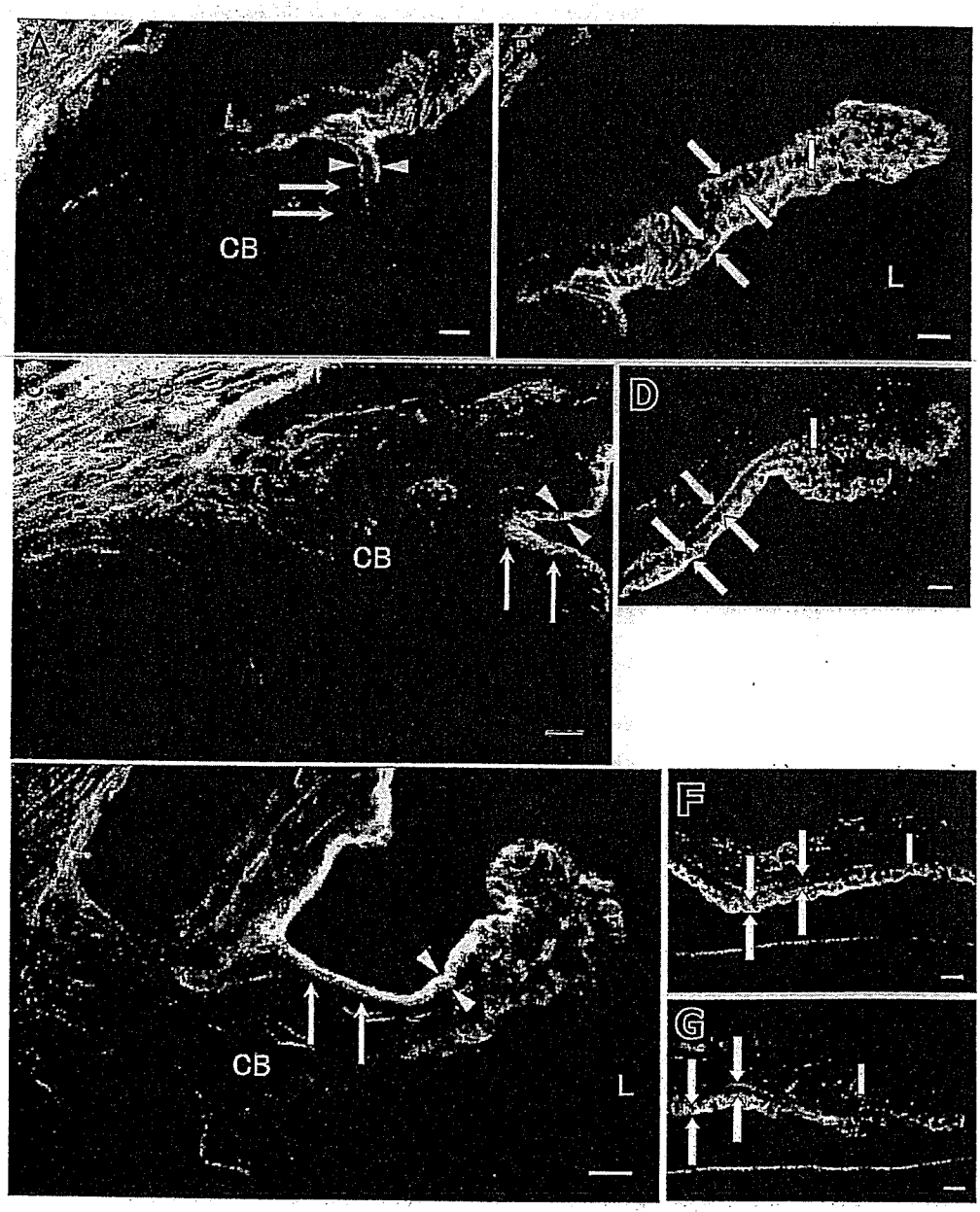

Fig. 2 AQP1 immunolocalization in iris and ciliary epithelial cells of postnatal rat eyes (*C* cornea, *CB* ciliary body, *I* iris, *L* lens). Vertical sections through anterior ocular segments dissected from P0, P7 and P14 rats were immunostained with anti-AQP1 antibody followed by FITC-labeled swine anti-rabbit immunoglobulin and then photographed under fluorescence optics. At P0 (**a**, **b**), both apical and basolateral plasma membranes of the inner plate cells corresponding to NPE cells in the anterior region of the ciliary body, displayed AQP1–IR (**a**, *arrowheads*), whereas outer plate cells corresponding to PE cells were AQP1-negative (**a**, *arrows*). In both layers of iris epithelial cells, both apical and basolateral plasma membranes were stained (**b**, *arrows*). At P7 (**c**, **d**) and P14 (**e**–**g**), the AQP1–IR pattern in the ciliary and iris epithelium was similar to that at P0 (**c**, **e**: *arrowheads* NPE, *arrows* PE; **d**, **g**: *arrows* anterior region of iris; **f**: *arrows* medial region of iris). Cornea was AQP1-positive throughout the postnatal stages (**c**). *Bars* 10 μm

Antibodies

Rabbit anti-rat AQP1 and AQP4 antibodies (Chemicon, Temecula, Calif.) were used. The specificities of these antibodies have been extensively examined by Western blot analysis in rodents (AQP1: Ward et al. 2001; Frigeri et al. 2004, AQP4: Yamamoto et al. 2001; Dalloz et al. 2003).

Immunofluorescence staining

For immunofluorescence staining, sections were rinsed in PBS (3×5 min each), treated with 10% normal swine serum in PBS for 10 min, and then incubated overnight at 4°C with either anti-AQP1 antibody (diluted 1:100) or anti-AQP4 antibody (diluted 1:20). All sections were rinsed in PBS (3×5 min each) and then incubated in swine anti-rabbit immunoglobulin coupled to fluorescein isothiocyanate (FITC; diluted 1:100; DakoCytomation, Glostrup, Denmark) for 1 h at room temperature. The above antibodies were all diluted in PBS containing 4% fetal calf serum, 0.1% sodium azide, and 0.1% Triton X–100. Sections were again rinsed in PBS (3×5 min each), mounted in glycerol containing 0.1% paraphenylenediamine to prevent bleaching, and examined with an Axioplan fluorescence microscope (Zeiss). Photomicrographs were taken by using 400 ASA Tri-X film (Kodak, Rochester, N.Y.).

To test the specificity of immunoreactivity (IR), control sections were processed in the same manner as described above, except that anti-AQP1 and anti-AQP4 antibodies were replaced with primary antibodies pre-adsorbed with either AQP1 or AQP4 oligopeptide (50 μg/ml diluted antibody; Chemicon), respectively, at 4°C for 4 h. These

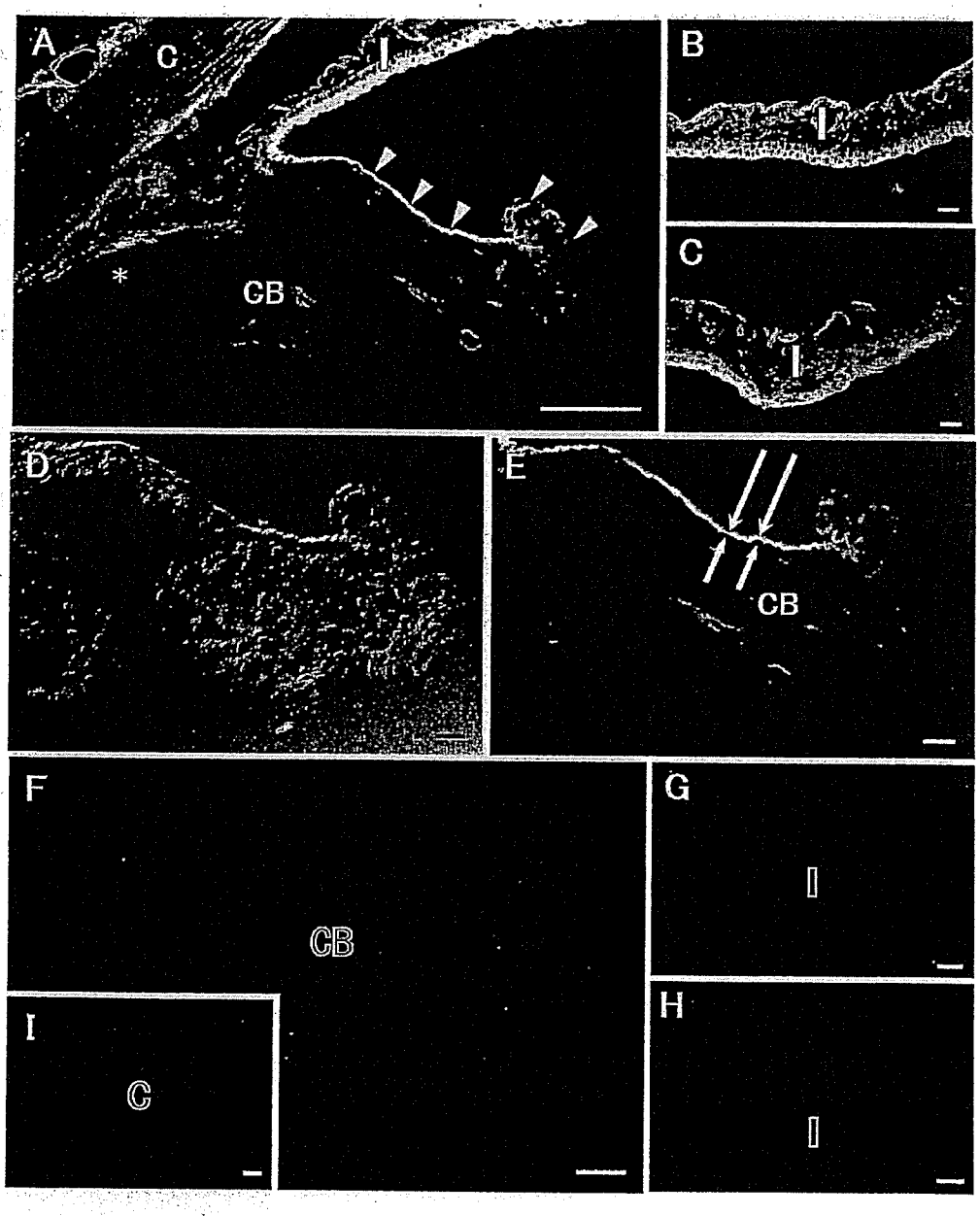

Fig. 3 AQP1 immunolocalization in iris and ciliary epithelial cells of PW8 rat eyes (*C* cornea, *CB* ciliary body, *I* iris, *asterisk* pars plana). Vertical sections through anterior ocular segments dissected from PW8 rats were immunostained with anti-AQP1 antibody followed by FITC-labeled swine anti-rabbit immunoglobulin and then photographed under Nomarski (**d**) and fluorescence (**a–c, e**) optics. AQP1–IR for epithelial cells in the iris (**a** posterior region, **b** medial region, **c** anterior region) and ciliary body (**a, d, e**) basically resembled that seen during developmental stages. In iris epithelial cells, both layers were AQP1-positive. In ciliary epithelial cells, only NPE cells localized anterior to the pars plicata were stained (**a**, *arrowheads*). AQP1–IR intensity was higher on the basolateral side (**e**, *long arrows*) than on the apical side (**e**, *small arrows*). In the remaining pars plicata and pars plana (**a**, *asterisk*), neither NPE cells nor PE cells were stained. Cornea was also AQP1-positive (**a**). **f–i** Pre-adsorption of anti-AQP1 antibody with antigenic peptide. PW8 rat anterior ocular segments were immunostained with anti-AQP1 antibody pre-adsorbed with AQP1-specific antigenic peptide. In ciliary (**f**) and iris (posterior region is not shown; **g** medial region, **h** anterior region) epithelium and in cornea (**i**), the AQP1–IR observed in **a–c** was completely abolished. *Bars* 10 μm

oligopeptides were equivalent to those used as immunogens to raise anti-AQP1 and anti-AQP4 antibodies.

Results

Prenatal AQP1 immunolocalization in iris and ciliary epithelial cells

At E13, no definitive AQP1–IR was observed in either the inner or outer plates of the optic cup (Fig. 1a,b). AQP1–IR first appeared at E15. At this stage, AQP–IR was confined to the anterior margin of the optic cup (Fig. 1c,d), where the inner plate of the optic cup showed more intense AQP1–IR than the outer plate, despite the outer and inner plates representing continuous tissues. In this region, AQP1–IR was observed all around the cell membrane. At E18, the anterior tip of the optic cup continued to grow along the lens anteriorly (Fig. 1e). At the same time, the iris and ciliary stroma began to form. The posterior part of the inner plate thickened markedly to form the neurosensory retina. AQP1–IR in the inner plate was more intense at E18 than at E15 (Fig. 1f). AQP1–IR in the outer plate also became more intense than at E15. However, AQP1–IR at E18 was again much more intense in the inner plate than in the outer plate. In the inner plate, although both apical and basolateral plasma membranes were stained, AQP1–IR intensity was higher on the basolateral side. At E20, when the iris became distinguishable from the ciliary body, AQP1–IR was observed in the most anterior region of the

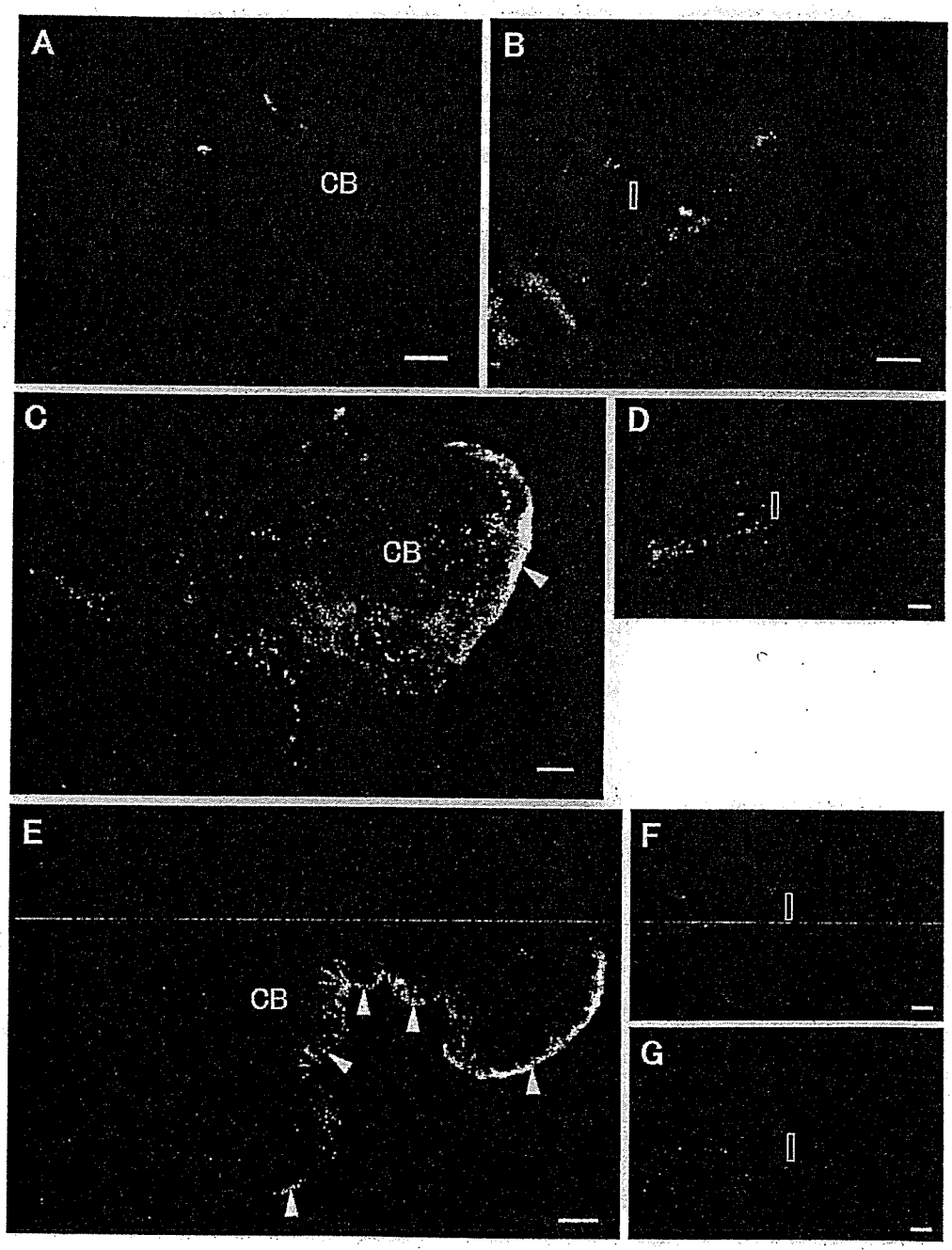

Fig. 4 AQP4 immunolocalization in iris and ciliary epithelial cells of postnatal rat eyes (*CB* ciliary body, *I* iris). Vertical sections through anterior ocular segments dissected from P0 (**a**, **b**), P7 (**c**, **d**), and P14 (**e**–**g**) rats were immunostained with anti-AQP4 antibody followed by FITC-labeled swine anti-rabbit immunoglobulin and then photographed under fluorescence optics. Little AQP4–IR was present in the ciliary body (**a**) or iris (**b**) at P0. Weak AQP4–IR was first observed on NPE cells of the immature pars plicata (**c**, *arrowhead*) at P7. AQP4–IR was more prominent at P14 than at P7 (**e**, *arrowheads*). At both P7 and P14, both iris epithelial layers (**d**, **g** anterior region; **f** medial region) were AQP4-negative. *Bars* 10 μm

ciliary body, in addition to the entire iris (Fig. 1g,h). At this stage, AQP1–IR intensity was significantly higher than at E15 or E18. AQP1–IR in the cornea was first seen at E15 and was observed throughout the embryonic stages (Fig. 1d,f,h).

Postnatal AQP1 immunolocalization in iris and ciliary epithelial cells

The iris and ciliary body remained structurally immature at birth (Fig. 2a). At P0, fold formation in the ciliary body remained incomplete. However, the ciliary body was more readily distinguishable from the iris at this stage than in the embryonic stages. In the anterior region of the ciliary body, both apical and basolateral plasma membranes of the inner plate cells corresponding to non-pigmented epithelial (NPE) cells, displayed AQP1-IR, whereas outer plate cells corresponding to pigmented epithelial (PE) cells showed no AQP1–IR (Fig. 2a). In both layers of the iris epithelial cells that were continuous with ciliary epithelial cells, both apical and basolateral plasma membranes were stained, but AQP1–IR intensity was lower in the anterior part of iris epithelium than in the posterior part (Fig. 2b). As development proceeded, the ciliary body formed more complex folds (Fig. 2c,e), and the iris extended at P7 and P14 (Fig. 2d,f,g). Patterns of AQP1–IR in the ciliary (Fig. 2c,e) and iris (Fig. 2d,f,g) epithelium at P7 and P14 basically resembled that at P0. AQP1–IR in the cornea was also observed throughout the postnatal stages (Fig. 2c).

At PW8, when development of the eyeball had been completed, AQP1–IR for epithelial cells in the iris and ciliary body was basically equivalent to that seen during the developmental stages. In iris epithelial cells, both layers were AQP1-positive (Fig. 3a–c). However, AQP1–IR was more intense in posterior epithelium compared to anterior epithelium. In ciliary epithelial cells, only NPE cells localized anterior to the pars plicata were stained (Fig. 3a). The intensity of AQP1–IR was higher on the basolateral side than on the apical side, again resembling observations made during development (Fig. 3d,e). In the remaining pars plicata and pars plana, neither NPE cells nor PE cells were stained (Fig. 3a). AQP1–IR was also observed in the cornea (Fig. 3a).

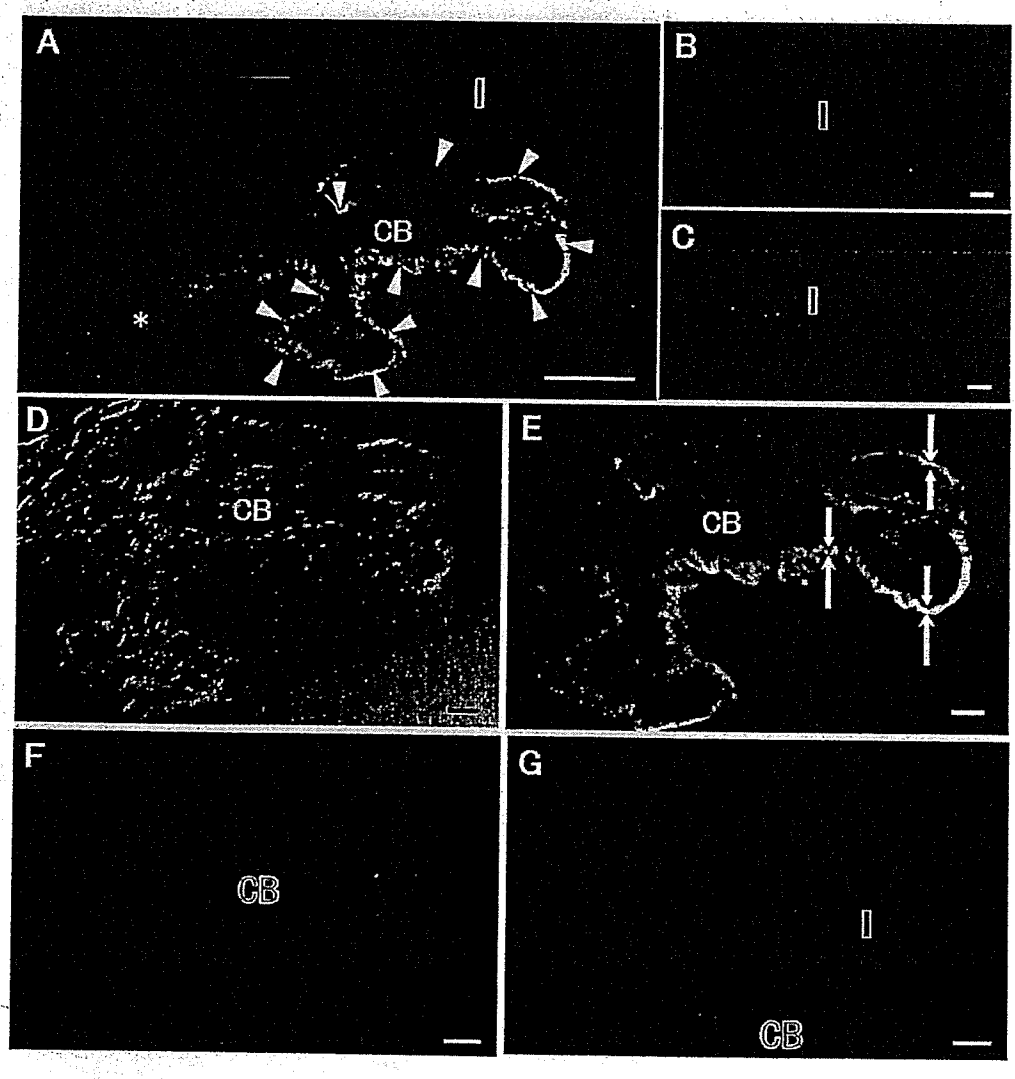

Fig. 5 AQP4 immunolocalization in iris and ciliary epithelial cells of PW8 rat eyes (*CB* ciliary body, *I* iris, *asterisk* pars plana). Vertical sections through anterior ocular segments dissected from PW8 rats were immunostained with anti-AQP4 antibody followed by FITC-labeled swine anti-rabbit immunoglobulin and then photographed under Nomarski (**d**) and fluorescence (**a–c, e**) optics. AQP4–IR was observed in the entire pars plicata region of the ciliary body (**a**, *arrowheads*). In this region, only NPE cells were AQP4-positive, not PE cells. AQP4-IR was observed only on the basolateral plasma membrane (**e**, *large arrows*), and the apical side was AQP4-negative (**e**, *small arrows*). In contrast, the pars plana region of the ciliary body did not show any significant AQP4–IR (**a**, *asterisk*). In the iris (**a**, posterior region; **b**, medial region; **c**, anterior region), only the posterior region continuous with NPE cells displayed weak AQP4–IR (**a**). **f–g** PW8 rat anterior ocular segment stained with anti-AQP4 antibody preadsorbed with antigenic peptide. Note that the AQP4–IR in ciliary and iris epithelium seen in **a** was completely abolished (**f**, ciliary body; **g**, posterior region of iris). *Bars* 10 μm

Pre- and postnatal AQP4 immunolocalization in iris and ciliary epithelial cells

No significant AQP4–IR was noted in the iris or ciliary body through perinatal stages up to P0 (Fig. 4a,b; prenatal period not shown). At P7, faint AQP4–IR was first observed on NPE cells of the immature pars plicata (Fig. 4c). By P14, AQP4–IR was more intense and extensive, and AQP4–IR in NPE cells in the pars plicata was unambiguously observed (Fig. 4e). At both P7 and P14, the two layers of iris epithelial cells were unstained (Fig. 4d,f,g).

At PW8, AQP4–IR was observed throughout the pars plicata. AQP4–IR in PE cells was negligible, and only NPE cells were stained (Fig. 5a). AQP4–IR in NPE cells was observed only in the basolateral plasma membrane and not on the apical side (Fig. 5d,e) or in the pars plana (Fig. 5a). In the iris (Fig. 5a–c), only the iris posterior region continuous with NPE cells displayed weak AQP4–IR (Fig. 5a).

Pre-adsorption of anti-AQP1 or anti-AQP4 antibody with antigenic peptide in PW8 rat eyes

When the primary antibodies against AQP1 and AQP4 were pre-adsorbed with the corresponding immunogenic peptides and then applied to PW8 anterior eye samples, all AQP1–IR and AQP4–IR observed at the ciliary body, iris, and cornea was completely abolished (AQP1, Fig. 3f–i; AQP4, Fig. 5f,g). Similarly, when E18 anterior eye samples were incubated with anti-AQP1 antibody pre-adsorbed with immunogenic AQP1 peptide, AQP1–IR both at the anterior tip of the optic cup and cornea was completely abolished (not shown).

Discussion

The present immunohistochemical study has revealed that iris and ciliary epithelial cells in the adult rat eye express both AQP1 and AQP4 with characteristic distribution patterns. Whereas AQP1–IR is localized to the entire iris and anterior ciliary body, AQP4–IR is localized solely to the ciliary body. On the basis of these AQP1 and AQP4 expression patterns, iris and ciliary epithelial cells can be divided into three regions (Fig. 6): region 1, including the major part of the iris, and expressing only AQP1; region 2, including the posterior iris and anterior pars plicata, expressing both AQP1 and AQP4; and region 3, the medial and posterior pars plicata, expressing AQP4 alone. These expression patterns may offer some insights into the mechanisms controlling intraocular fluid transport. First of all, the present study has confirmed and further extended the findings of previous investigations that AQP is present on iris epithelial cells (Nielsen et al. 1993; Hamann et al. 1998). The results of our study support the idea that iris epithelial cells, in addition to ciliary epithelial cells, are

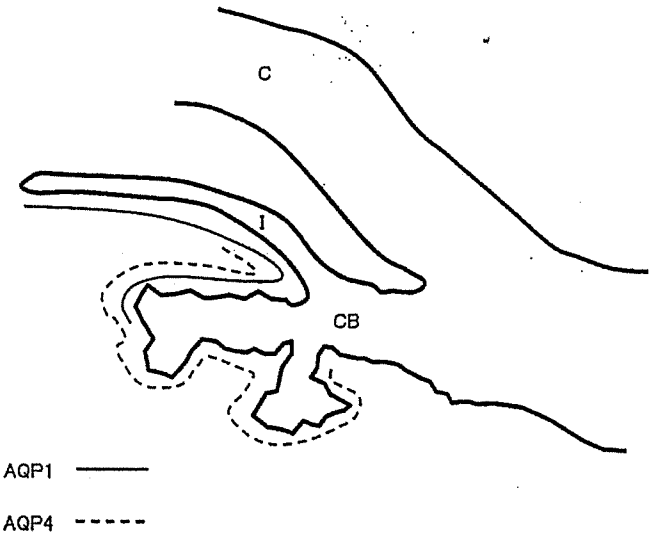

Fig. 6 Representation of expression patterns for AQP1 (*solid line*) and AQP4 (*dotted line*) in iris and ciliary epithelial cells in PW8 rat eyes. Iris and ciliary epithelia are divided into three regions depending on AQP1 and AQP4 expression patterns. Region 1 includes the major part of the iris and expresses only AQP1. Region 2 includes the posterior region of the iris and anterior pars plicata and expresses both AQP1 and AQP4. Region 3 includes the medial and posterior pars plicata and expresses AQP4 alone (*C* cornea, *CB* ciliary body, *I* iris)

involved in the secretion of the aqueous humor (Green and Pederson 1973). Since the precise role of the iris in regulating aqueous humor volume remains unclear, the present findings are expected to provide clues for further analysis of this issue. Secondly, the characteristic AQP1 and AQP4 expression patterns raise the possibility that ciliary epithelial cells in regions 2 and 3 differ with respect to their ability to secrete aqueous humor, although ciliary epithelial cells in these two regions appear morphologically indistinguishable. Studies have yet to determine the way that each of these two regions contributes to aqueous humor secretion within the ciliary body, in which aqueous humor is most actively secreted. Thirdly, no significant AQP1 or AQP4 expression has been detected in the pars plana in this study, consistent with the localization of Na–K–ATPase and Na–K–Cl–cotransporter, both of which are considered to be closely associated with aqueous humor secretion. Both Na–K–ATPase and Na–K–Cl–cotransporter are reportedly more abundant in the pars plicata than in the pars plana (Ghosh et al. 1991; Dunn et al. 2001). The present study thus provides a molecular basis for aqueous humor secretion through an analysis of AQP distribution. Fourthly, the localization of AQP1 and AQP4 also differs significantly at the cellular level. Our results for AQP1 expression on both the apical and basolateral plasma membranes of both layers of iris epithelial cells and ciliary NPE cells confirm the findings of Hamann et al. (1998). Recent studies have shown that cultured NPE cells actively transport liquid in an apical–to–basolateral direction in the absence of PE cells (Patil et al. 2001). AQP1 on both apical and basolateral plasma membranes may play important

roles in transporting water within ciliary NPE cells. In contrast, the present findings on AQP4 expression differ from those of previous studies (Hamann et al. 1998), in which AQP4 reactivity has been demonstrated on both the apical and basolateral plasma membranes of NPE cells. Although the reasons for this discrepancy remain unclear, variable expression of AQP isoforms as described above may contribute to the precise volume regulation of aqueous humor. AQP1–IR has also been found in the cornea from E15 through to adulthood. The observation of AQP1–IR at PW8 in the present study is consistent with that reported previously (Hamann et al. 1998).

The essential role of AQP molecules in regulating aqueous humor balance has been demonstrated by the generation of mice lacking AQP1 and/or AQP4 (Zhang et al. 2002). Significant decreases in IOP have been seen in these mice. Interestingly, aqueous humor secretion is significantly decreased in mice lacking AQP1 alone and also in mice lacking both AQP1 and AQP4, indicating a major role for AQP1 in fluid transport in the murine eye (Zhang et al. 2002). In contrast, humans with complete hereditary deficiency of AQP1 show no significant IOP abnormalities and instead display only a disorder in maximal urinary concentrating ability (King et al. 2001). This may be attributable to the presence of various compensatory mechanisms among AQP isoforms, such as functional redundancy, at least in the eye. Species differences may also warrant consideration.

AQP molecules in iris and ciliary epithelial cells thus appear to play important roles in regulating aqueous humor turnover and thereby in regulating IOP. In future, the manipulation of aqueous humor secretion may be achievable by regulating the kinetics of AQP molecules by using factors regulating AQP1 and AQP4 activity (Patil et al. 1997b; Han et al. 1998; Han and Patil 2000). The present study may represent a starting point for designing novel therapies to treat disorders caused by impaired IOP regulation, such as glaucoma.

The present study also examined the expression of AQP1 and AQP4 in developing rats. AQP1–IR was detected as early as E15, whereas AQP4–IR was first observed at P7. AQP4–IR density increased with development, possibly reflecting increases in the requirement of aqueous humor secretion in the area. Taken together, developing iris and ciliary epithelium expressed only AQP1 during the embryonic and early postnatal stages, but expressed both AQP1 and AQP4 after birth. AQP1 is known to be abundant in the choroid plexus throughout fetal development in the rat, indicating the presence of AQP1-mediated water transport in cerebrospinal fluid secretion during embryonic stages (Bondy et al. 1993). Similarly, AQP1 in the eye appears to play an important role in water transport during the prenatal period. Interestingly, when fold formation of the ciliary body is still immature during embryogenesis, AQP1 appears to be more abundantly expressed in the iris than in the ciliary epithelial primordium. This pattern contrasts with that in the adult eye, where the ciliary body is the dominant site of AQP expression. These results indicate that the iris epithelium is more active in secreting aqueous humor compared with ciliary epithelium during embryonic life. Indeed, one previous study has suggested that AQP1 expression in iris epithelium is related to the regulation of aqueous humor volume (Hasegawa et al. 1994).

IOP in the early prenatal stage has been considered to be maintained primarily by the growing vitreous body (Beebe 1986). If this is really the case, active fluid transport by the ciliary epithelium may play little if any role in this regard (Beebe 1986). The present results, however, suggest that AQP1 found in the inner plate is involved in fluid secretion, even in the prenatal period. Indeed, in chicks, early secretion of aqueous humor from the embryonic stages has been demonstrated (Latker and Beebe 1984; Linser and Plunkett 1989; Reichman and Beebe 1992). Secretion of aqueous humor during the embryonic stages is further supported by experiments on mouse embryos in which the administration of carbonic anhydrase inhibitors suppressed aqueous humor secretion and caused microphthalmia (Scott et al. 1984). The presence of functional tight junctions in rat ciliary epithelium as early as E18 also supports its involvement in secretion (Arguillere et al. 1986). The findings of the present study thus provide a molecular basis for aqueous humor secretion from the iris and ciliary epithelial primordium during the prenatal period.

In conclusion, the study reported here has confirmed that AQP molecules play important roles in the regulation of aqueous humor secretion in rats, in both mature and developing eyes. These results provide a basis for understanding the molecular mechanisms underlying the regulation of normal intraocular fluid balances and offer insights into the pathophysiology of disorders involving the impairment of intraocular fluid balance.

References

Arguillere P, Patey A, Hirsch M (1986) Quantitative analysis of tight junctions during ciliary epithelium development. Exp Eye Res 42:239–248

Beebe DC (1986) Development of the ciliary body: a brief review. Trans Ophthalmol Soc UK 105:123–130

Bondy C, Chin E, Smith BL, Preston GM, Agre P (1993) Developmental gene expression and tissue distribution of the CHIP28 water-channel protein. Proc Natl Acad Sci USA 90:4500–4504

Calamita G, Bishai WR, Preston GM, Guggino WB, Agre P (1995) Molecular cloning and characterization of aqpZ, a water channel from *Escherichia coli*. J Biol Chem 270:29063–29066

Caprioli J (1992) The ciliary epithelia and aqueous humor. In: Hart WM (ed) Adler's physiology of the eye. Mosby, St. Louis, pp 228–247

Chrispeels MJ, Agre P (1994) Aquaporins water channel proteins of plant and animal cells. Trends Biochem Sci 19:421–425

Dalloz C, Sarig R, Fort P, Yaffe D, Bordais A, Pannicke T, Grosche J, Mornet D, Reichenbach A, Sahel J, Nudel U, Rendon A (2003) Targeted inactivation of dystrophin gene product Dp71: phenotypic impact in mouse retina. Hum Mol Genet 12:1543–1554

Dunn JJ, Lytle C, Crook RB (2001) Immunolocalization of the Na–K–Cl cotransporter in bovine ciliary epithelium. Invest Ophthalmol Vis Sci 42:343–353

Frigeri A, Nicchia GP, Balena R, Nico B, Svelto M (2004) Aquaporins in skeletal muscle: reassessment of the functional role of aquaporin-4. FASEB J 18:905–907

Ghosh S, Hernando N, Martin–Alonso JM, Martin–Vasallo P, Coca–Prados M (1991) Expression of multiple Na+,K(+)–ATPase genes reveals a gradient of isoforms along the nonpigmented ciliary epithelium: functional implications in aqueous humor secretion. J Cell Physiol 149:184–194

Green K, Pederson JE (1973) Aqueous humor formation. Exp Eye Res 16:273–286

Hamann S, Zeuthen T, La Cour M, Nagelhus EA, Ottersen OP, Agre P, Nielsen S (1998) Aquaporins in complex tissues: distribution of aquaporins 1–5 in human and rat eye. Am J Physiol 274: C1332–C1345

Han Z, Wax MB, Patil RV (1998) Regulation of aquaporin-4 water channels by phorbol ester-dependent protein phosphorylation. J Biol Chem 273:6001–6004

Han Z, Patil RV (2000) Protein kinase A-dependent phosphorylation of aquaporin-1. Biochem Biophys Res Commun 273:328–332

Hasegawa H, Lian SC, Finkbeiner WE, Verkman AS (1994) Extrarenal tissue distribution of CHIP28 water channels by in situ hybridization and antibody staining. Am J Physiol 266: C893–C903

King LS, Choi M, Fernandez PC, Cartron JP, Agre P (2001) Defective urinary-concentrating ability due to a complete deficiency of aquaporin-1. N Engl J Med 345:175–179

Latker CH, Beebe DC (1984) Developmental changes in the blood-ocular barriers in chicken embryos. Exp Eye Res 39:401–414

Linser PJ, Plunkett JA (1989) A role for carbonic anhydrase in early eye morphogenesis. Invest Ophthalmol Vis Sci 30:783–785

Matsuzaki T, Tajika Y, Tserentsoodol N, Suzuki T, Aoki T, Hagiwara H, Takata K (2002) Aquaporins : a water channel family. Anat Sci Int 77:85–93

Nielsen S, Smith BL, Christensen EI, Agre P (1993) Distribution of the aquaporin CHIP in secretory and resorptive epithelia and capillary endothelia. Proc Natl Acad Sci USA 90:7275–7279

Patil RV, Saito I, Yang X, Wax MB (1997a) Expression of aquaporins in the rat ocular tissue. Exp Eye Res 64:203–209

Patil RV, Han Z, Wax MB (1997b) Regulation of water channel activity of aquaporin 1 by arginine vasopressin and atrial natriuretic peptide. Biochem Biophys Res Commun 238:392–396

Patil RV, Han Z, Yiming M, Yang J, Iserovich P, Wax MB, Fischbarg J (2001) Fluid transport by human nonpigmented ciliary epithelial layers in culture: a homeostatic role for aquaporin-1. Am J Physiol Cell Physiol 281:C1139–C1145

Reichman EF, Beebe DC (1992) Changes in cellular dynamics during the development of the ciliary epithelium. Dev Dyn 193:125–135

Scott WJ Jr, Lane PD, Randall JL, Schreiner CM (1984) Malformations in nonlimb structures induced by acetazolamide and other inhibitors of carbonic anhydrase. Ann N Y Acad Sci 429:447–456

Stamer WD, Snyder RW, Smith BL, Agre P, Regan JW (1994) Localization of aquaporin CHIP in the human eye: implications in the pathogenesis of glaucoma and other disorders of ocular fluid balance. Invest Ophthalmol Vis Sci 35:3867–3872

Verkman AS (2003) Role of aqaporin water channels in eye function. Exp Eye Res 76:137–143

Ward DT, Yau SK, Mee AP, Mawer EB, Miller CA, Garland HO, Riccardi D (2001) Functional, molecular, and biochemical characterization of streptozotocin-induced diabetes. J Am Soc Nephrol 12:779–790

Yamamoto N, Yoneda K, Asai K, Sobue K, Tada T, Fujita Y, Katsuya H, Fujita M, Aihara N, Mase M, Yamada K, Miura Y, Kato T (2001) Alterations in the expression of the AQP family in cultured rat astrocytes during hypoxia and reoxygenation. Mol Brain Res 90:26–38

Zhang D, Vetrivel L, Verkman AS (2002) Aquaporin deletion in mice reduces intraocular pressure and aqueous fluid production. J Gen Physiol 119:561–569

Graefe's Arch Clin Exp Ophthalmol
(2004) 242:792–799

LABORATORY INVESTIGATION

DOI 10.1007/s00417-004-0935-6

Michael Völker
Kei Shinoda
Helmut Sachs
Helmut Gmeiner
Thorsten Schwarz
Konrad Kohler
Werner Inhoffen
Karl Ulrich Bartz-Schmidt
Eberhart Zrenner
Florian Gekeler

In vivo assessment of subretinally implanted microphotodiode arrays in cats by optical coherence tomography and fluorescein angiography

Received: 23 December 2003
Revised: 17 February 2004
Accepted: 26 March 2004
Published online: 4 June 2004

M. Völker · K. Shinoda (✉) · H. Gmeiner · T. Schwarz · K. Kohler · W. Inhoffen · K. U. Bartz-Schmidt · E. Zrenner · F. Gekeler
University Eye Hospital,
Calwerstrasse 7/1, 72076 Tübingen,
Germany
e-mail: shinodak@uni.de
Tel.: +49-7071-2987074
Fax: +49-7071-295568

H. Sachs
University Eye Hospital,
Franz-Josef-Strauß-Allee 11,
93053 Regensburg, Germany

Abstract *Background:* Following multiple promising investigations into restoration of vision in degenerative retinal disease by implantation of a sub- or epiretinal prosthesis, the step to clinical use in humans is impending. In this study we intended to establish optical coherence tomography (OCT) and fluorescein angiography (FA) first in research animals for noninvasive assessment of the condition of the posterior pole of eyes after intraocular implant surgery. *Methods:* Three adult cats that had undergone subretinal implant surgery were evaluated by OCT and FA between 1 and 470 days postoperatively. Eight adult cats served as control. In addition histology was performed. *Results:* In all three cats OCT demonstrated stable positioning of the implants in the subretinal space during the complete examination period. Transient retinal edema was found in the early postoperative period but decreased during follow-up. The retina over the implants was well attached at all times in cats 1 and 2; however, in cat 3 localized retinal detachment was demonstrated. FA showed intact retinal vasculature over the subretinal implant in high detail without interference from choroidal background fluorescence. *Conclusions:* OCT and FA have been fruitfully applied to cats to assess the morphological and circulatory conditions of the neuroretina and of its interface with the subretinal implant. The techniques may therefore provide a tool for objective, noninvasive in vivo evaluation of eyes that have undergone subretinal implant surgery, both in research animals and in humans.

Introduction

Numerous efforts are currently under way to develop retinal prostheses to replace degenerated photoreceptors in diseases such as retinitis pigmentosa (RP) and age-related macular degeneration [1, 3, 6, 16, 17]. In these diseases epi- or subretinal implants are intended to electrically stimulate the remaining cell populations [7, 11, 14].

Several animal investigations [4, 12, 15, 17, 18] have reported the stable fixation of subretinal implants within the subretinal space (SRS), and no major undesired reactions such as cell proliferation, inflammation, or retention of subretinal fluid have been reported in various histological studies even after several years [9, 12, 15, 18]. Up to now, no objective morphological data in vivo about retinal tissue and its interface with the implant have been available. Adequate methods for such purposes are mandatory because effective signal transduction can only be achieved if close, stable contact is obtained between the implant and the neurosensory retina. Histological post mortem examinations, however, show inherent limitations.

The purpose of this study was to ascertain the feasibility of optical coherence tomography (OCT) and fluorescein angiography (FA) in animals to assess the biocompatibility of subretinally implanted microphotodiode arrays (MPDAs). We report stable fixation of the MPDA

in the SRS and tight contact between the MPDA and the retina by OCT, and intact retinal vasculature and circulation by FA.

Methods

Animals

Three healthy adult cats were examined by OCT on days 1, 8, 17, and 51 after subretinal surgery in cat 1, and on day 99 in cats 2 and 3. Additionally, cat 3 was examined on day 470. FA was performed on day 51 in cat 1 and on day 470 in cat 3. Eight age-matched adult cats were examined by OCT as control. All animal experiments adhered to the "Principles of laboratory animal care" (NIH publication No. 85–23, revised 1985), the OPRR Public Health Service Policy on the Humane Care and Use of Laboratory Animals (revised 1986), and the U.S. Animal Welfare Act, as amended, as well as the local commission for animal welfare.

Surgical procedure

Surgery was done under intubation narcosis (1.8% isoflurane) in the left eye with pupils dilated. The high reflectivity of the tapetum lucidum required no endoillumination, thereby enabling two-port vitrectomy. Two sclerotomies were made 6.0 mm posterior to the limbus. After partial vitrectomy between sclerotomy and area centralis, a 31-gauge cannula (Visitec, Sarasota, FL) was used to create a localized retinal bleb by injecting a small amount of balanced salt solution; the bleb was enlarged by injecting Healon (Pharmacia, Stockholm, Sweden). A 2.5-mm retinotomy was then made circumferentially at the temporal portion on the bleb. The MPDA was introduced into the vitreous cavity with an intravitreal end-gripping forceps. After the MPDA had been inserted through the retinotomy into the SRS, it was forwarded ca. 1 mm outside of the created bleb under the retina near the area centralis.

MPDA specifications

The subretinally implanted prototype of a MPDA consisted of 48 single photodiodes which were grouped in fours to stimulate the retina via 12 titanium nitrite electrodes. The device measured 50 µm in thickness and 2 mm in diameter; it was electrically active and functioning (for a description of similar devices see [19]).

Optical coherence tomography

After intramuscular anesthesia and pupil dilation, cats were placed in front of the Optical Coherence Tomograph (Zeiss-Humphrey, Dublin, CA; software version A 6.1, 1997) in a stereotactic apparatus which ensured mechanical stability of the animal. The principle of the OCT has been described previously [13]. The following tomographic images were obtained in all animals (Fig. 1a): (1) a long vertical scan of approximately 6 to 8 mm along the axis including the MPDA, the optic disc, and the retinotomy site, and (2) vertical and horizontal (orthogonal to the vertical) scans of approximately 4 mm length over the MPDA. A digital video image was taken to visualize the OCT scan's position on the retina. For measurements of the MPDA's diameter in horizontal direction the eye length was adjusted to 21.50 mm (manufacturer's recommendation).

Thickness and horizontal length measurements (in micrometers and millimeters, respectively) were performed using the instrument's built-in algorithm; accuracy of the automatic detection of the borders of the neurosensory retina was checked individually. The area comprised of the retina above the implanted MPDA was calculated by standard image-processing software which counted the number of pixels in the picture exported from the OCT software. To adjust for slightly differing scan lengths, mean retinal thickness was calculated by division of the area (in pixels×pixels) by the horizontal length in pixels and then transformed into micrometers. Mean retinal thickness was used to assess retinal tissue changes over time.

Fundus photography and fluorescein fundus angiography

FA was performed in the standard manner [5] with a fundus camera (TRC-50IA; TOPCON, Paramus, NJ). Photographs were taken with a black-and-white digital camera (Kodak Megaplus Model 1.4,

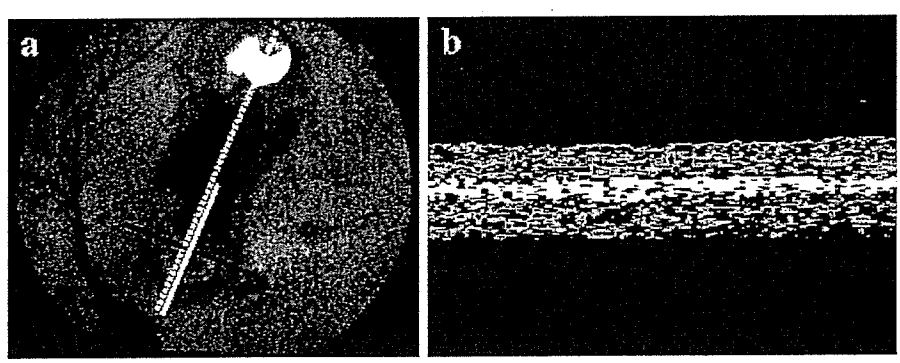

Fig. 1 **a** Black-and-white digital photograph with the three OCT scan paths (one long and two short scans) routinely used in all cats. Stable positioning of the microphotodiode array in the subretinal space near the area centralis is demonstrated. The retina appears attached in all areas. Peripherally from the microphotodiode array a black spot occurred in all cats in the area where the bleb had been formed during surgery to introduce the implant into the subretinal space. The area of high reflectance in the periphery of the black spot corresponds to the intentional retinal break exposing the cat's tapetum lucidum layer. **b** Illustrative horizontal OCT image of a control animal. The cat retina showed a more homogeneous structure than a human retina. The wider white band most possibly corresponds to the complex of tapetum lucidum and choriocapillaris

Eastman Kodak, Rochester, NY), after injection of 10 mg/kg of 10% fluorescein into a cephalic vein.

Histologic assessments of the retinae

After enucleation the anterior segment including the lens was removed and the posterior eye cups with the retina in place were fixed overnight at 4°C in 4% paraformaldehyde in 100 mM phosphate buffer, pH 7.4. Following the fixation a fine slit was made through the retina directly in front of the implant and the device was carefully removed out of its tissue pocket. The eye cup was then embedded in paraffin by standard protocols; radial 5-µm sections were cut, collected on slides, and examined microscopically after staining with hematoxylin and eosin.

Results

General remarks on OCT and FA imaging in cats

Due to the highly reflective tapetum lucidum, brightness ranges of the instrument had to be reduced to allow localization of the OCT beam on the video image. The OCT power and sensitivity had to be reduced by a factor of approximately 4. All other settings were comparable to those for human examinations.

One illustrative OCT image of a control animal is shown in Fig. 1b. In general, the cat retina had a more homogeneous appearance than the human retina where ideally the nerve fiber layer, the inner and outer plexiform layer, and the photoreceptor layer can be differentiated [13]. The subretinal layers in the cat showed much greater reflectivity than human eyes. The wider white band most possibly corresponds to the complex of retinal pigment epithelium (RPE), tapetum lucidum, and choriocapillaris. Mean retinal thickness of horizontal scans in the control animals was 215 µm±13.4 µm.

The highly reflective and intransmissible MPDA caused a total extinction of the OCT beam, inhibiting any evaluation of the structures behind the implant (e.g., Fig. 2).

Cat 1

Funduscopy revealed the MPDA in the desired position under the retina at all examination dates. The MPDA itself appeared intact. Neither persistent bleeding nor proliferative changes were observed at the posterior pole at any time. The retina appeared flat in all regions, including the area over the MPDA, except for small folds in the area where the bleb had been formed. The appearance of a black subretinal spot extending from the edge of the MPDA to the area where the bleb had been formed (Fig. 1a) did not alter over time. Localized retinal edema was suspected over the MPDA during the early postoperative period, although judgment of retinal alterations was made more difficult by the high reflectivity of the MPDA. Irregular retinal thickness was observed over the MPDA with a prominent thinning in the leading one third of the implant at all examination times.

On day 1 floating opacities in the vitreous cavity decreased the quality of fundus photographs, causing a low-reflection area behind them (Fig. 2). However, OCT images were obtainable. The retina over the MPDA was attached from day 1; it was detached in the area where the bleb had been formed but reached flatness also in this area on day 51 (Fig. 2). In the area of the black spot thinning of subretinal layers in OCT was observed (Fig. 2).

Irregular thickness of the neurosensory retina over the MPDA in the vertical scan was demonstrated; in the horizontal direction no such irregularity occurred (Fig. 2).

The range of the retinal thickness over the MPDA in the horizontal scan was 170–227 µm, 135–214 µm, 161–220 µm, and 136–175 µm on days 1, 8, 17, and 51, respectively. Mean retinal thickness was 195 µm, 190 µm, 195 µm, and 155 µm, respectively. Thickness in the vertical scan was 145–231 µm, 146–243 µm, and 110–214 µm on days 8, 17, and 51, respectively. Mean retinal thickness was 185 µm, 189 µm, and 161 µm, respectively. The development of mean retinal thickness above the MPDA is shown in Fig. 3.

FA on day 51 showed well-demarcated hypofluorescence corresponding to the MPDA and the black spot; at the border of the latter area also hyperfluorescence occurred. Otherwise no pathologic findings—such as leakage, neovascularization, or partial or total obstruction of vessels—were detectable (Fig. 4).

Cat 2

Funduscopy revealed an attached retina over the MPDA on day 1. In analogy to cat 1 we found an initial edema over the MPDA and a partial retinal thinning. On day 99 OCT scans showed retinal attachment over the MPDA (Fig. 5). Retinal conditions of the posterior pole including the site where the retinal bleb had been formed and the retinotomy site were comparable to cat 1. Retinal thickness over the MPDA ranged from 122 µm to 196 µm, corresponding to a mean retinal thickness of 163 µm (Fig. 3)

Cat 3

Funduscopy revealed no pathologic findings, in analogy to cats 1 and 2. On day 99 OCT scans of the retina over the MPDA showed a no-signal area between retina and MPDA extending over the central one third of the MPDA (Fig. 6). This may have corresponded to focal retinal detachment in this area that was not detectable by funduscopy. The retina in the area of the bleb was attached

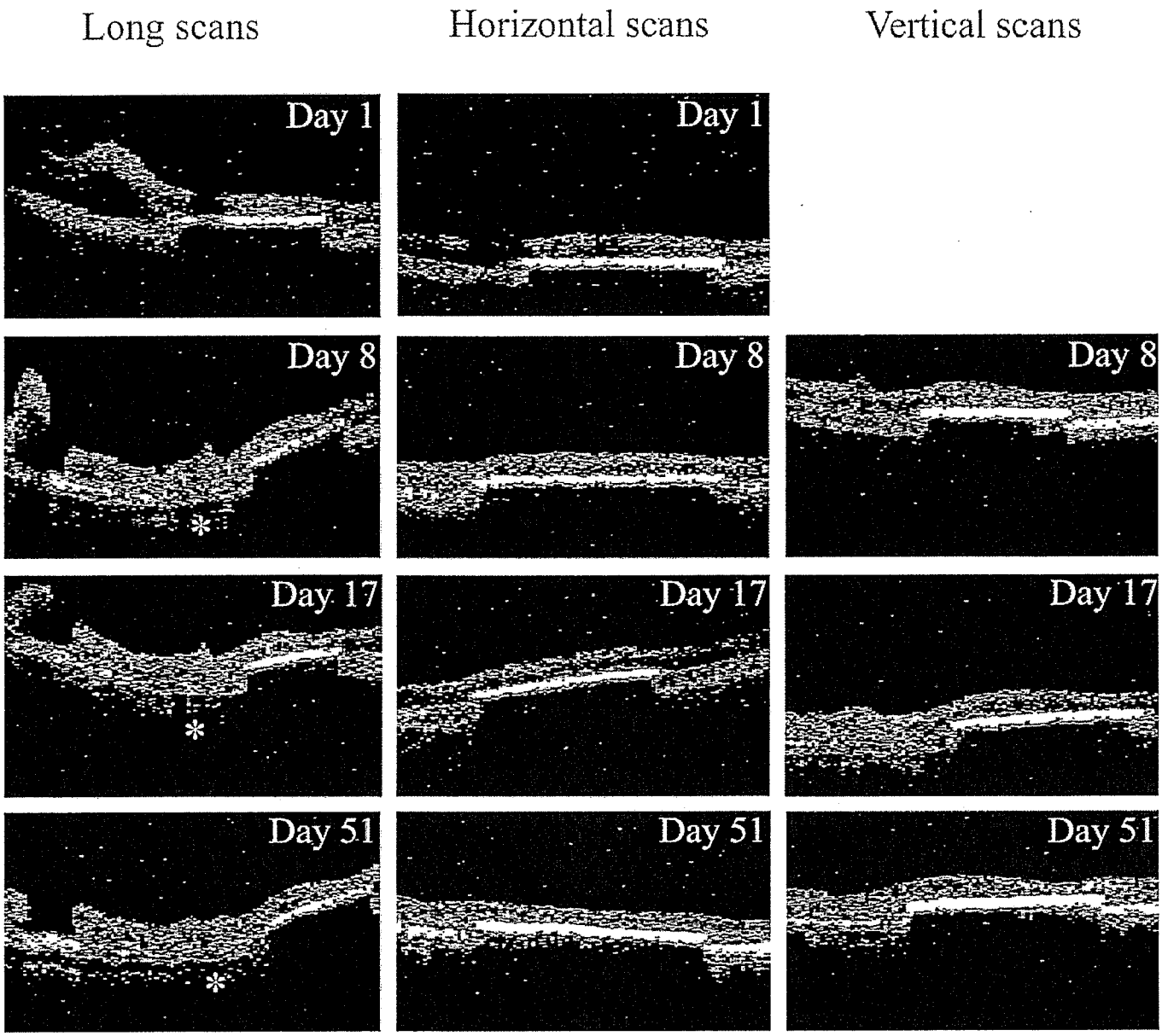

Fig. 2 OCT scans of cat 1 on days 1, 8, 17, and 51 (raw data). The *columns* show the different scan paths: vertical long scans of ca. 6–8 mm in the first column, detailed horizontal scans over the microphotodiode array of ca. 4 mm length in the second column, and detailed vertical scans of ca. 4 mm over the microphotodiode array in the third column. The *rows* show the scans at different time points. The subretinally implanted microphotodiode array, which is highly reflective and intransmissible, is observed as a homogeneously flat and white band with well-defined margins and homogeneous thickness, causing total extinction of the OCT beam, inhibiting any evaluation of the structures behind it. Retinal attachment over the microphotodiode array occurred on day 1. Low reflections located at a different position in the pictures in the first row were artifacts caused by vitreous opacities observed only in the early postoperative period. The irregularities in retinal thickness in the vertical scans which were not detectable in the horizontal scans decreased over the whole examination period. Retinal attachment has occurred in all areas at latest on day 51 in the area where the bleb has been formed during surgery and the area of the intentional retinal break. Thinning of subretinal layers appeared next to the implant in the area corresponding to the black spot seen in Fig. 1 (*)

(Fig. 6). Retinal thickness over the MPDA ranged from 95 µm to 190 µm, corresponding to a mean retinal thickness of 174 µm (Fig. 3).

On day 470 OCT scans of the retina over the MPDA still showed a no-signal area between retina and MPDA (Fig. 6). The retina in the area of the bleb remained (Fig. 6). Retinal thickness over the MPDA ranged from 98 µm to 184 µm, corresponding to a mean retinal thickness of 144 µm (Fig. 3).

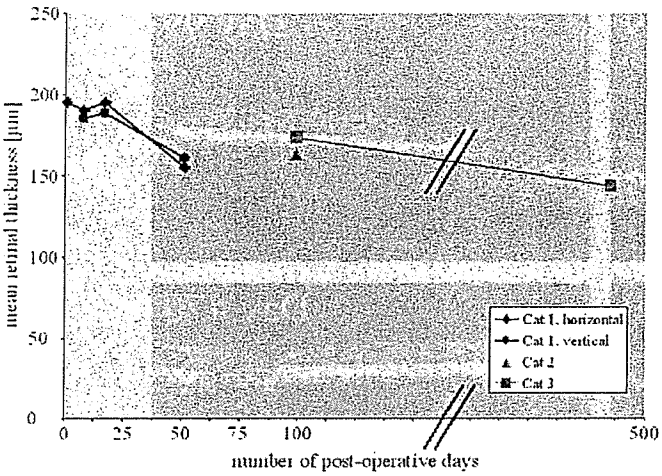

Fig. 3 Development of mean retinal thickness over time. In cat 1 mean retinal thickness over the implant decreased after an initial plateau of 17 days following surgery, in the vertical as well as in the horizontal scans. On day 99 mean retinal thickness over the implant in cats 2 and 3 was approximately the same as in cat 1 on day 51. In cat 3 mean retinal thickness further decreased between day 99 and day 470

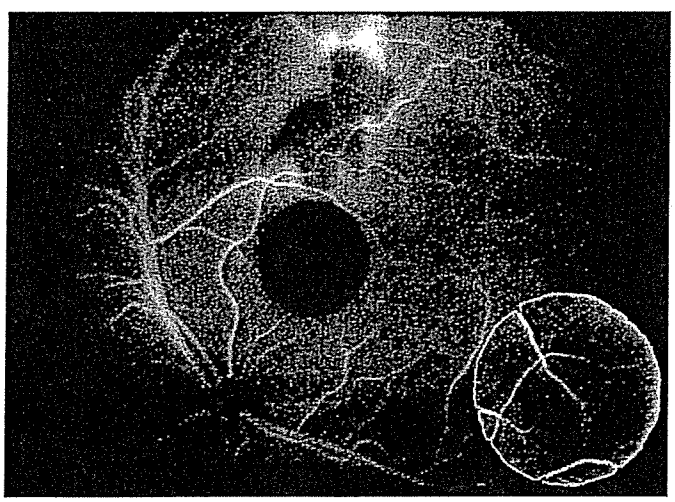

Fig. 4 Fluorescein angiography (FA) in cat 1 on day 51. The area over the microphotodiode array (*inset*) was photographed with different exposure time due to the high reflectance of the microphotodiode array. FA demonstrates no abnormal findings in the areas over the microphotodiode array and over the black spot, appearing in the area where the subretinal bleb was formed during surgery. Due to the blockage of background fluorescence by the microphotodiode array assessment of retinal vasculature was possible in high detail

In FA on day 470 no pathologic findings were detected, in analogy to cat 1, except a small area of hyperfluorescence at the upper border of the area where the bleb had been formed during surgery (Fig. 7).

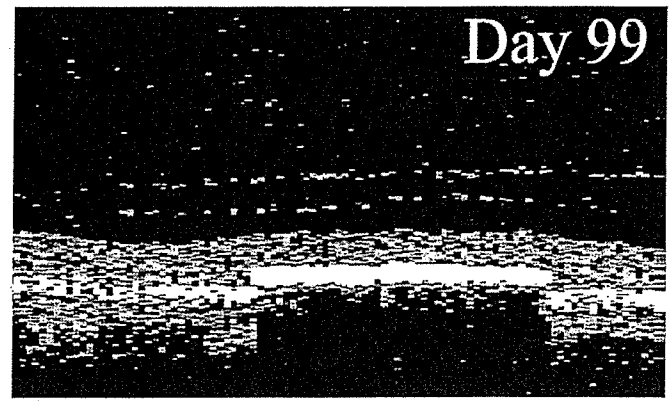

Fig. 5 OCT scans of cat 2 on day 99 (raw data). The retina over the microphotodiode array seemed totally attached and in close contact to the microphotodiode array. Two parallel lines in the vitreous cavity could correspond to the posterior vitreous cortex

Remarks on horizontal measurements of the MPDA by OCT

The MPDA's diameter ranged from 1.87 mm to 2.34 mm, corresponding to an under- or overestimation of 6.5% or 17%, respectively. Only 2 of 10 measurements were below 2 mm.

Surgical procedure

All surgeries were performed as planned with no serious adverse events resulting in stable positioning of the MPDA under the retina in the desired position. No complications (such as endophthalmitis and proliferative vitreoretinopathy) were observed during the follow-up period. Because of the anatomy of the cat eye's the following modifications to submacular surgery as practiced in humans were made: (1) only two sclerotomies were placed, (2) no posterior vitreous detachment (PVD) was created, (3) to maintain an opening for the introduction of the subretinal device into the retinal bleb viscoelastic material was introduced into the SRS, (4) from our previous experience no laser photocoagulation around the retinotomy was applied, (5) no tamponading substances, i.e., expanding gas or silicone oil, were used.

Histology

At 158 days postoperatively up to four rows of outer nuclear layer (ONL) cells were present in the retinal area overlying the implant along its margin. The number of these ONL cells decreased steadily from the margin towards the central regions of the implant, down to a single row of cells (Fig. 8a). The preservation of the inner retina varies, but the general retinal architecture was well pre-

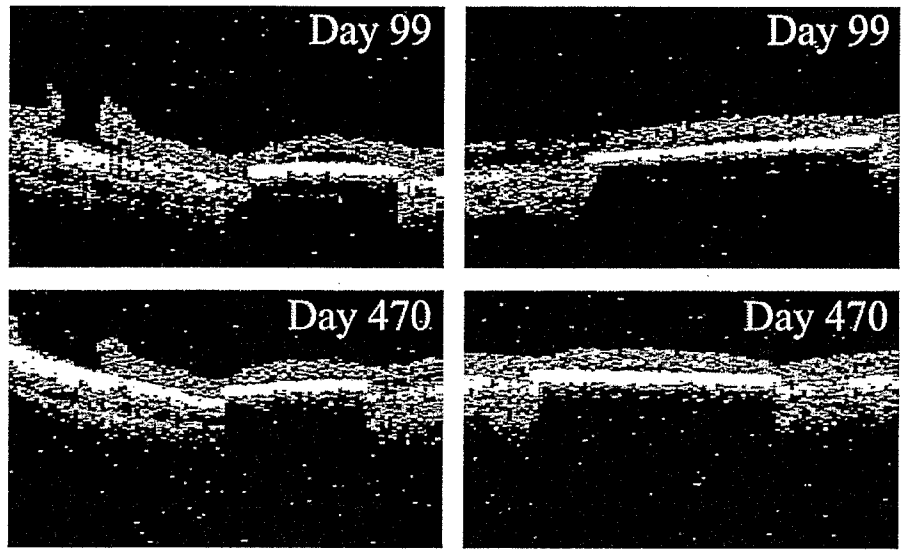

Fig. 6 OCT scans of cat 3 on days 99 and 470 (raw data). The *columns* show the different scan paths: vertical long scans of ca. 6–8 mm in the first column, detailed horizontal scans over the microphotodiode array of ca. 4 mm length in the second column. The *rows* show the scans at different time points. On day 99 the long scan demonstrates localized retinal detachment over the central one third of the microphotodiode array which is also visible in the horizontal scan. On day 470 this localized retinal detachment could still be observed, although to a lesser extent

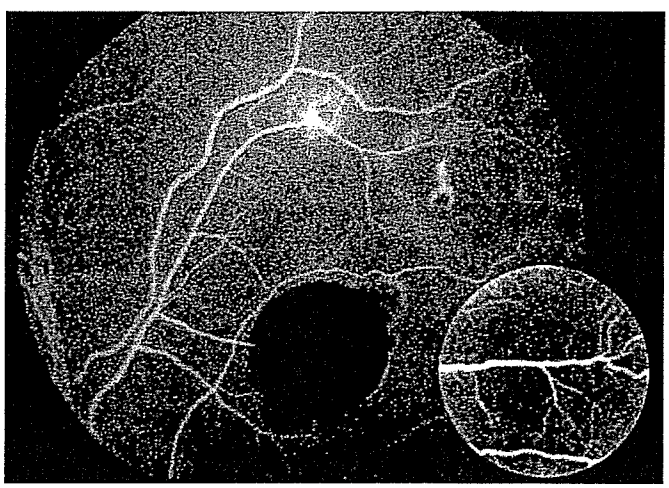

Fig. 7 Fluorescein angiography (FA) in cat 3 on day 470. FA demonstrates normal retinal vasculature in the posterior pole and in the area over the microphotodiode array (see *inset*)

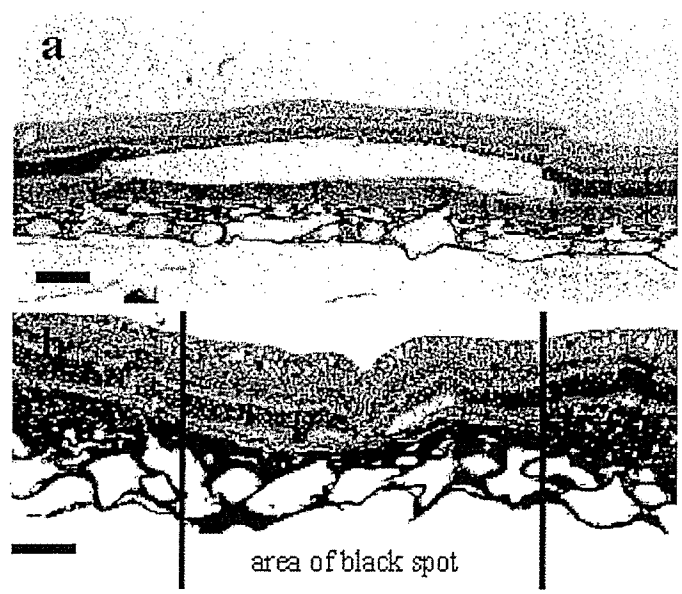

Fig. 8 Histological sections 158 days after implantation in cat 1. **a** The implant was removed prior to sectioning but its former position is clearly visible by a cavity located between the neurosensory retina and the retinal pigment epithelium/tapetum lucidum (*asterisk*). Note the well-preserved neuronal retina overlying the implant. **b** The black spot along the implantation channel where the tapetum lucidum has disappeared and the black-pigmented choroid is now located directly adjacent to the translucent retina. The tapetum lucidum laterally to the channel is marked by an *asterisk* (calibration bar is 200 μm)

served over the entire implant and the neuronal network of horizontal, amacrine, and ganglion cells was without substantial deficits. Hyperplasia of Müller glia was occasionally found, but minimal, in those areas where at least one row of ONL cells remained. The tissue bag surrounding the implant was coated with a fibrous membrane less than 10 μm thick.

Histology of the area of the black spot revealed a total loss of the tapetum lucidum (Fig. 8b). As a consequence

the pigmented choroid was visible in this area along the implantation channel.

Discussion

The feasibility of OCT examinations in cats which have undergone subretinal implant surgery using commercially available machines has been demonstrated successfully. This study provides to the authors' knowledge the first analysis of the cat fundus by OCT.

All images obtained were of superb quality without artifacts from foreign bodies as seen, for example, in computer tomography or ultrasound sonography. The possibility of performing OCT under these conditions might be of clinical importance in cases where localization or measurement of intraocular foreign bodies is required. Since the device totally blocked any imaging of details behind it, in the RPE or choroid OCT is applicable only to subretinal and not to epiretinal implants.

OCT imaging has several advantages over other imaging techniques and histological studies. First, it is noninvasive, thus allowing longitudinal studies. It can be applied to humans who have undergone subretinal implant surgery where stringent assessment of the retina over and around the device and of its stable positioning is of critical importance. Second, OCT is an in vivo technique, measuring tissue structures in living conditions, and it therefore does not suffer from artifactual changes in tissue morphology during histological preparation. Third, it is sufficiently sensitive to detect relatively small changes in retinal thickness. Fourth, OCT imaging is fast. Fifth, OCT images are digitized and are therefore objectively quantifiable for statistical analysis.

In cat 1 mean retinal thickness over the MPDA had decreased by day 51, suggesting resolution of postsurgical edema, and reached a level which was also found in cat 2 and cat 3 on day 99. This is in good accordance with observation by biomicroscopy and functional analyses where higher thresholds to elicit cortical responses following subretinal electrical stimulation were found in acute than in chronic experiments. Mean retinal thickness over the MPDA of cats 1–3 falls within the range of the control animals in the early postoperative period but falls outside during later examinations. The progressive thinning observed in all animals during the later stage is due to degeneration of outer segments which is proven by histology in Fig. 8, where an almost complete lack of this layer is demonstrated in contrast to a well-preserved inner retina. The deterioration of the photoreceptor layer, which is not vascularized, is due to the lack of nutrition from the underlying retinal pigment epithelium and choroid. As there is no debris found on either the front or the back surface of the implant an apoptotic mechanism seems to be most likely. Apoptotic cell death of photoreceptors has been described in degenerative retinal disease such as age-related macular degeneration.

In cat 1 retinal attachment over the MPDA's region was observed by OCT as early as day 1. It is speculated that the persistent subretinal fluid observed in cat 3 at all examinations is associated with lack of direct contact of this space with the RPE, with retention of, for example, the viscoelastic material over the MPDA, with the influence of the coating of the device, or with some tractional force of remaining vitreous cortex. Posterior vitreous cortex (as seen in Fig. 6) can be left undetected by OCT. In the current study creation of PVD was omitted due to strong attachment of the posterior vitreous cortex in the cat eye. Although successful submacular surgery without PVD creation has been reported in humans [8], strict removal of posterior vitreous can be considered important in the case of subretinal implantation in human eyes to prevent complications related to vitreous traction.

Irregularities in retinal thickness appeared in the long and vertical scans in cat 1 at all examination dates while not appearing in the horizontal scans. It might be associated with the physical force used while forwarding the MPDA within the SRS outside of the bleb.

OCT, in accordance with histology, showed no adverse tissue reactions such as cell proliferation or inflammation within the retina or around the implant in this study or in precursor studies [15]. This is in slight contrast to previous reports where cell proliferation, especially of Müller cells, has been demonstrated above and beneath the implanted device [10]. Differences, however, exist in animal models, surgical procedure, implant design and material, and method of histological preparation.

The slight variation of the horizontal length measurement from the actual size of the MPDA is attributed to off-center location of the examination beam. The overestimation of the MPDA's diameter by approximately 17% is attributed to the fact that the eye length was not individually assessed in our cats (instead, 21.5 mm was used).

Since MPDAs are totally intransmissible for the wavelengths used, FA can assess pure retinal circulation over subretinal implants to detect pathological conditions of retinal vasculature—ischemia, neovascularization, vasculitis, leakage, etc. FA in our animals demonstrated no abnormality of retinal vasculature, neither on day 51 nor on day 470. This finding further supports the assumption that the persistent subretinal fluid in cat 3 is associated with retained fluid rather than leakage from retinal vessels.

Black spots following subretinal surgery in cats have been previously reported [12]. Apparent thinning of subretinal layers in this area has been found by OCT in this study (e.g., Fig. 2). Histologically we were able to prove that the tapetum lucidum is absent or partially interrupted in this area, making the pigmented choroids visible through the unpigmented RPE. The alteration in

thickness of the highly reflective layer in the OCT image could provide in vivo proof of impairment of the tapetum lucidum, although OCT imaging of highly reflective layers is generally believed to be less reliable. Considering the fact that these spots were observed as soon as the first postoperative day, direct surgical trauma is a likely cause, although chemical injury by viscoelastic material cannot be excluded.

Since little experience has yet been gathered with subretinal implants in humans [2], much remains to be learned about the reaction of the (degenerated) human retina to subretinal implants. Certainly, the posterior pole of humans with implants has to be monitored closely, including not only the retina over the MPDA but also the site of the intentional retinal break and the area where the bleb has been formed during surgery. OCT so far provides the only noninvasive and objective technique to judge these conditions in humans over a prolonged period of time. In cases of implant failure evaluation of the retinal condition in regard to attachment to the MPDA, trauma, or edema can help to find the optimal treatment.

Acknowledgements Support of this study was provided by the Keio Gijuku Fukuzawa Memorial Fund for the Advancement of Education and Research and the German Federal Ministry of Education and Research (BMBF), grant 01 IN 502 A. The authors thank Chiaki Kato and Mitsuko Agarie for excellent technical advice. The collaboration with our partners in Stuttgart (IMS and IPE) and Reutlingen (NMI), who delivered the subretinal implants and were helpful in solving many technical problems, is appreciated.

References

1. Chow AY, Chow VY (1997) Subretinal electrical stimulation of the rabbit retina. Neurosci Lett 225:13–16
2. Chow AY, Packo KH, Pollack JS, Schuchard RA (2003) Subretinal artificial silicon retina microchip implantation in retinitis pigmentosa patients: long term follow-up. Invest Ophthalmol Vis Sci abstract, annual meeting
3. Eckhorn R, Stett A, Schanze T, Gekeler F, Schwahn H, Zrenner E, Wilms M, Eger M, Hesse L (2001) [Physiological functional evaluation of retinal implants in animal models]. Ophthalmologe 98:369–375
4. Gekeler F, Schwahn HN, Stett A, Kohler K, Zrenner E (2001) Subretinal microphotodiodes to replace photoreceptor-function—a review of the current state. In: Doly M, Droy M-T, Christen Y (eds) Vision, sensations et environnement, Irvinn, Paris, pp 77–95
5. Hill DW, Young S (1975) Infrared angiography of the cat fundus oculi. Arch Ophthalmol 93:131–133
6. Humayun MS, de Juan EJ, Weiland JD, Dagnelie G, Katona S, Greenberg R, Suzuki S (1999) Pattern electrical stimulation of the human retina. Vision Res 39:2569–2576
7. Humayun MS, Prince M, de Juan EJ, Barron Y, Moskowitz M, Klock IB, Milam AH (1999) Morphometric analysis of the extramacular retina from postmortem eyes with retinitis pigmentosa. Invest Ophthalmol Vis Sci 40:143–148
8. Kambara C, Inoda S, Shimizu Y, Tanabe K, Tuckwell HC (2000) [Optical coherence tomographic features after surgery for rhegmatogenous retinal detachment with macular involvement]. Jpn J Clin Ophthalmol 54:327–330
9. Kohler K, Hartmann JA, Werts D, Zrenner E (2001) [Histological studies of retinal degeneration and biocompatibility of subretinal implants]. Ophthalmologe 98:364-368
10. Loewenstein JI, Rizzo JF, Montezuma SR (2002) Implantation of subretinal polyimide in Yucatan pigs. Invest Ophthalmol Vis Sci abstract, annual meeting
11. Milam AH, Li ZY, Fariss RN (1998) Histopathology of the human retina in retinitis pigmentosa. Prog Retin Eye Res 17:175–205
12. Pardue MT, Stubbs EB, Jr., Perlman JI, Narfstrom K, Chow AY, Peachey NS (2001) Immunohistochemical studies of the retina following long-term implantation with subretinal microphotodiode arrays. Exp Eye Res 73:333–343
13. Puliafito CA, Hee MR, Lin CP, Reichel E, Schuman JS, Duker JS, Izatt JA, Swanson EA, Fujimoto JG (1995) Imaging of macular diseases with optical coherence tomography. Ophthalmology 102:217–229
14. Santos A, Humayun MS, de Juan EJ, Greenburg RJ, Marsh MJ, Klock IB, Milam AH (1997) Preservation of the inner retina in retinitis pigmentosa. A morphometric analysis. Arch Ophthalmol 115:511–515
15. Schwahn HN, Gekeler F, Kohler K, Kobuch K, Sachs HG, Schulmeyer F, Jakob W, Gabel VP, Zrenner E (2001) Studies on the feasibility of a subretinal visual prosthesis: data from Yucatan micropig and rabbit. Graefes Arch Clin Exp Ophthalmol 239:961–967
16. Wyatt J, Rizzo JF (1996) Ocular implants for the blind. IEEE Spectrum 33:47–53
17. Zrenner E (2002) Will retinal implants restore vision? Science 295:1022–1025
18. Zrenner E, Stett A, Weiss S, Aramant RB, Guenther E, Kohler K, Miliczek K-D, Seiler MJ, Haemmerle H (1999) Can subretinal microphotodiodes successfully replace degenerated photoreceptors? Vision Res 39:2555–2567
19. Zrenner E, Gekeler F, Gabel VP, Graf HG, Graf M, Guenther E, Haemmerle H, Hoefflinger B, Kobuch K, Kohler K, Nisch W, Sachs H, Schlosshauer B, Schubert M, Schwahn H, Stelzle M, Stett A, Troeger B, Weiss S (2001) [Subretinal microphotodiode array as replacement for degenerated photoreceptors?]. Ophthalmologe 98:357–363

Suppression of Ocular Inflammation in Endotoxin-Induced Uveitis by Blocking the Angiotensin II Type 1 Receptor

Norihiro Nagai,[1,2,3] *Yuichi Oike,*[1,3] *Kousuke Noda,*[2] *Takashi Urano,*[3] *Yoshiaki Kubota,*[3] *Yoko Ozawa,*[1,2] *Hajime Shinoda,*[2] *Takashi Koto,*[1] *Kei Shinoda,*[2] *Makoto Inoue,*[2] *Kazuo Tsubota,*[2] *Kenji Yamashiro,*[4] *Toshio Suda,*[3] *and Susumu Ishida*[1,2]

PURPOSE. To examine whether the angiotensin II type 1 receptor (AT1-R) signaling plays a role in ocular inflammation in endotoxin-induced uveitis (EIU).

METHODS. EIU was induced in C57BL/6 mice by a single intraperitoneal injection of 150 μg lipopolysaccharide (LPS). Tissue localization, mRNA expression, and protein levels of AT1-R in murine retinas were examined by immunohistochemistry, RT-PCR, and Western blot analyses, respectively. Telmisartan, an AT1-R antagonist widely used as an antihypertensive agent, was administered intraperitoneally at a dose of 10 mg/kg daily for 5 days until the injection of LPS. Twenty-four hours after administration, leukocyte adhesion to the retinal vasculature was evaluated with a concanavalin A lectin perfusion-labeling technique. Retinal mRNA and protein levels of intercellular adhesion molecule (ICAM)-1 were examined by RT-PCR and ELISA, respectively. Protein concentration and inflammatory cells in the aqueous humor were also measured.

RESULTS. Retinal vessels were positive for AT1-R. In mice with EIU, retinal AT1-R mRNA and protein levels were significantly increased when compared to the normal control. EIU animals also showed significant increases in the number of inflammatory cells infiltrating the anterior chamber and adhering to the retinal vessels and in retinal ICAM-1 levels. Administration of telmisartan to EIU mice resulted in significant suppression of retinal ICAM-1 expression and leukocyte adhesion and infiltration compared with vehicle treatment. Protein concentration in the aqueous humor of telmisartan-treated EIU mice tended to be lower than that of vehicle-treated EIU mice, but the difference was not statistically significant.

CONCLUSIONS. AT1-R signaling blockade inhibited retinal ICAM-1 upregulation and leukocyte adhesion and infiltration in the EIU model. These results suggest the potential use of an AT1-R antagonist as a therapeutic agent to reduce ocular inflammation. (*Invest Ophthalmol Vis Sci.* 2005;46:2925–2931) DOI:10.1167/iovs.04-1476

From the [1]Laboratory of Retinal Cell Biology and the Departments of [2]Ophthalmology and [3]Cell Differentiation, Keio University School of Medicine, Tokyo, Japan; and the [4]Department of Ophthalmology, Kobe City General Hospital, Kobe, Japan.

Submitted for publication December 15, 2004; revised March 30, 2005; accepted April 19, 2005.

Disclosure: **N. Nagai**, Boehringer Ingelheim (F); **Y. Oike**, None; **K. Noda**, None; **T. Urano**, None; **Y. Kubota**, None; **Y. Ozawa**, Boehringer Ingelheim (F); **H. Shinoda**, None; **T. Koto**, Boehringer Ingelheim (F); **K. Shinoda**, None; **M. Inoue**, None; **K. Tsubota**, None; **K. Yamashiro**, None; **T. Suda**, None; **S. Ishida**, Boehringer Ingelheim (F)

The publication costs of this article were defrayed in part by page charge payment. This article must therefore be marked "*advertisement*" in accordance with 18 U.S.C. §1734 solely to indicate this fact.

Corresponding author: Susumu Ishida, Laboratory of Retinal Cell Biology, Department of Ophthalmology, Keio University School of Medicine; 35 Shinanomachi, Shinjuku-ku, Tokyo 160-8582, Japan; ishidasu@sc.itc.keio.ac.jp.

Endotoxin-induced uveitis (EIU) is an animal model of acute ocular inflammation induced by the administration of lipopolysaccharide (LPS), a component of Gram-negative bacterial outer membranes.[1–3] Because uveitis frequently leads to severe vision loss and blindness with retinal vasculitis, retinal detachment, and glaucoma, it is important to elucidate further the mechanisms in the development of ocular inflammation. LPS enhances the expression of various inflammatory mediators, such as interleukin (IL)-6,[3,4] tumor necrosis factor (TNF)-α,[5] prostaglandin E2,[6] and monocyte chemotactic protein (MCP)-1,[7] as well as the production of nitric oxide,[6] all of which contribute to the development of EIU, resulting in the breakdown of the blood–ocular barrier and in the infiltration of leukocytes. For the first phase of leukocyte infiltration, cell adhesion to vascular endothelium is essential, in which adhesion molecules play major roles.[8] Among various adhesion molecules, intercellular adhesion molecule (ICAM)-1 and its receptor, lymphocyte function-associated antigen (LFA)-1, are necessary for the development of EIU.[8–10] Although EIU was originally used as a model of anterior uveitis, increasing evidence shows that it also involves inflammation in the posterior segment of the eye with recruitment of leukocytes that adhere to the retinal vasculature and infiltrate the vitreous cavity.[11,12]

The renin–angiotensin system is a major controller of systemic blood pressure. Angiotensin II, the effector molecule of the system, has two cognate receptors: angiotensin II type 1 receptor (AT1-R) and AT2-R.[13,14] Because major functions of angiotensin II are mediated by AT1-R, its antagonists are widely used to treat patients with hypertension and cardiovascular diseases. Recently, several studies have demonstrated the diverse biological functions of angiotensin II as a modulator of angiogenesis, vascular remodeling, and inflammation.[15–20] As an inflammatory mediator, angiotensin II enhances vascular permeability through prostaglandins and vascular endothelial growth factor,[17] and contributes to the recruitment of inflammatory cells by inducing chemokines and adhesion molecules.[18,19] Moreover, angiotensin II directly induces the proliferation and differentiation of inflammatory cells per se.[20] AT1-R blockade is reported to attenuate such inflammatory processes effectively.[17–19] Recent studies have demonstrated the prevention of EIU by suppressing inflammatory mediators including IL-6, TNF-α, cyclooxygenase (COX)-2, inducible nitric oxide synthase (iNOS), and MCP-1.[5–7,21–24] However, it is not clear whether AT1-R blockade is effective in reducing ocular inflammation. In the current study we show for the first time the anti-inflammatory effects of an AT1-R antagonist, telmisartan, on ocular inflammation in a murine model of EIU.

METHODS

Animals and Induction of EIU

C57BL/6 mice (7–10 weeks old; SLC, Shizuoka, Japan) were used. All animal experiments were conducted in accordance with the ARVO